**Title**

The LINC complex contributes to heterochromatin organisation and transcriptional gene silencing in plants

**Running title**

LINC complex and heterochromatin

**Authors :**

Axel POULET [1, 3, 4], Céline DUC [1, 4], Maxime VOISIN [1], Sophie DESSET [1], Sylvie TUTOIS [1], Emmanuel VANROBAYS [1], Matthias BENOIT [2], David E. EVANS [3], Aline V. PROBST [1] and Christophe TATOUT [1, *]

[1] UMR CNRS 6293 INSERM U1103 Clermont Université, Clermont-Ferrand, France

[2] Sainsbury Laboratory Cambridge, University of Cambridge, Cambridge CB2 1LR, UK

[3] Department of Biological and Medical Sciences, Oxford Brookes University, Oxford OX3 0BP, UK

[4] These authors contributed equally to this work.

[*] Address correspondence to Christophe Tatout, Laboratory of Genetics, Reproduction and Development, 10 Avenue Blaise Pascal, TSA 60026 - CS 60026, 63178 Aubière Cedex, France (Tel. +33 473407406, Fax. +33 473407406, e-mail: christophe.tatout@univ-bpclermont.fr) ORCID ID: 0000-0001-5215-2338.

**Keywords:** nuclear organisation, 3D imaging, lamina, LINC complex, heterochromatin, chromocentre

## Summary Statement

The plant LINC complex contributes to heterochromatin position at the nuclear periphery and to maintenance of transcriptional gene silencing.


## Abstract

The LInker of Nucleoskeleton and Cytoskeleton (LINC) complex is an evolutionary well-conserved protein bridge connecting the cytoplasmic and nuclear compartments across the nuclear membrane. While recent data support its function in nuclear morphology and meiosis, its implication in chromatin organisation has not been studied in plants. Here 3D imaging methods have been used to investigate nuclear morphology and chromatin organisation in interphase nuclei of the model plant *Arabidopsis thaliana,* in which heterochromatin cluster in conspicuous chromatin domains called chromocentres. Chromocentres form a repressive chromatin environment contributing to transcriptional silencing of repeated sequences, a general mechanism needed for genome stability. Quantitative measurements of 3D position of chromocentres indicate their close proximity to the nuclear periphery but that their position varies with nuclear volume and can be altered in specific mutants affecting the LINC complex. Finally we propose that the plant LINC complex contributes to proper heterochromatin organisation and positioning at the nuclear periphery, since its alteration is associated with the release of transcriptional silencing as well as decompaction of heterochromatic sequences.


## Introduction

In eukaryotic cells, the Nuclear Envelope (NE), consisting of a double membrane interrupted by nuclear pores, delimits the nuclear compartment from the cytoplasm. The NE has many functions beyond the one of a simple barrier (Graumann and Evans, 2013; Méjat and Misteli, 2010). It regulates exchanges between the nucleus and the cytoplasm *via* the nuclear pore complex (Adams and Wente, 2013; Tamura et al., 2010), organises telomeres, connects the centromere to the centrosome during cell division, and bridges nucleus and cytoskeleton *via* the LInker of Nucleoskeleton and Cytoskeleton (LINC) complex (Crisp et al., 2006). During the past few years, the LINC complex has been shown to play a central role in many NE functions. The LINC complex senses stimuli from the outside of the cell and transmits information through the cytoskeleton to the nucleus, contributes to nuclear migration required to position the nucleus within the cell, and can interact with nucleoskeleton components such as lamins inside the nucleus. Lamins can form direct or indirect contacts with chromatin in many organisms (Mattout et al., 2015), and the nucleoskeleton and the NE are therefore expected to participate in the position of chromatin within the nucleus (Bickmore and van Steensel, 2013). The NE is an elastic structure and can expand or

retract upon constraints from within or from outside the nucleus. Indeed, alterations in the nucleoskeleton or the cytoskeleton have been associated with modifications of nuclear shape and size. Lamin mutants, such as those observed in the premature aging syndrome Hutchinson-Gilford progeria syndrome (HGPS) display ghost-like instead of spherical nuclear shapes (Shumaker et al., 2006). In the cytoskeleton, actin, microtubules and actomyosin have all been shown to participate in nuclear shape (Gerlitz and Bustin, 2011). Most plant cells do not display spherical nuclei and the functional significance of nuclear reshaping toward elongated or lobed nuclei remains a question of debate. Two main hypotheses have been proposed (Webster et al., 2009): first, nuclear reshaping may modify the nuclear rigidity needed for nuclear movement. Second, nuclear reshaping may induce chromatin reorganisation, which in turn modifies gene expression. In light of this second hypothesis, it could be envisaged that nuclear structures that determine nuclear shape would also impact on chromatin organisation and function. In addition to nuclear shape, nuclear size has been shown to be modulated independently of genome size through cellular factors in a range of organisms (Levy and Heald, 2010; Neumann and Nurse, 2007). These studies also highlighted the independency between ploidy level and karyoplasmic ratio, defined by the ratio between nuclear size and cell volume. Similar results have been reported in plants (Bourdon et al., 2012; Jovtchev et al., 2006; Sugimoto-Shirasu and Roberts, 2003).

Plants are amenable models to study nuclear organisation as natural variations in nuclear morphology occur in various tissues such as epidermis, trichomes, root hairs (Qian et al., 2009; Traas et al., 1998) or during seed formation (van Zanten et al., 2011) as well as in mutants in which the nuclear envelope or lamin-like components are altered (Dittmer et al., 2007; Goto et al., 2014b; Janski et al., 2012; Tamura and Hara-Nishimura, 2011; Zhou et al., 2012). Plants encode a LINC complex consisting of SUN (SAD1-UNC-84 HOMOLOGY) (Graumann and Evans 2010; Graumann et al. 2014) and KASH (Klarsicht / Anc-1 / Syne homology) proteins including WIPs (WPP domain-interacting proteins), SINEs (SUN-interacting nuclear envelope) and TIK (Zhou et al. 2012; Graumann et al. 2014; Zhou, Graumann, and Meier 2015). Furthermore, possible candidates for lamin-like proteins have been identified and are known as CROWDED NUCLEI (CRWN) (Dittmer et al., 2007; Wang et al., 2013) and KAKU4 (Goto et al., 2014b). Strikingly, *sun, wip, kaku4* and *crwn* mutants all display nuclear shape and/or nuclear size modifications suggesting that mechanical constraints such as those applied by the cytoskeleton at the NE may be released in mutant backgrounds (Dittmer et al., 2007; Goto et al., 2014a; Oda and Fukuda, 2011; van Zanten et al., 2011; Zhou et al., 2012). Finally, the SUN-WIP-WIT2-myosin XI-i complex and CRWN1 were proposed to independently determine elongated nuclear shape, highlighting the function of cytoskeleton and nucleoskeleton in nuclear morphology (Zhou, Groves, and Meier 2015). However, to date it is not known whether plants deficient in nuclear envelope or lamina components would

also show altered chromatin organisation or whether in turn, mutants that affect the organisation of chromatin would impact ~~on~~ nuclear size and shape.

To address these questions, three cell types displaying contrasted nuclear organisation, namely guard cells, pavement cells and root hair cells have been chosen to investigate both nuclear shape and chromatin organisation. For the latter, we took advantage of the fact that repressed chromatin domains called heterochromatin can easily be tracked in Arabidopsis interphase nuclei in which they form compact and dense chromatin domains called chromocentres (Fransz et al., 2002). Nuclei were classed according to their tissues of origin using 3D quantitative parameters such as sphericity and elongation and we show that in wild type most of the chromocentres are located close to the nuclear periphery. Loss-of function mutants for lamina, LINC complex components or chromatin remodelers and modifiers were then evaluated for their impact on nuclear morphology as well as heterochromatin organisation and function in these three specific cell types using quantitative parameters and 3D-Fluorescence *in situ* hybridisation (3D-FISH) as well as transcriptional silencing by RT-qPCR. Plants deficient for components of the LINC complex, such as KASH (*wifi*) and SUN (*sun1 sun4 sun5* triple mutant) show altered nuclear shape, increased distance of chromocentres from the nuclear periphery, altered heterochromatin organisation and reactivation of transcriptionally silent repetitive sequences. Taken together, this study reveals a critical role for the LINC complex in heterochromatin positioning and function.

## Results

### Different cell types show quantitative variations in nuclear organisation

Plants are well known for their variation in genome size but also display a wide range of nuclear morphologies. For example in the model species *Arabidopsis thaliana* hypocotyls and trichomes (Traas et al., 1998), root hairs (Sugimoto-Shirasu et al., 2005) and pollen tubes (Dittmer et al., 2007; Grob et al., 2014; Wang et al., 2013) have been used to illustrate variations in cell and nuclear morphogenesis. Here, we chose three different cell types displaying distinct nuclear features to characterise their nuclear shapes and chromatin organisation (Fig. 1A). Cotyledon epidermal cells consisting mainly of guard cells (GC), with round nuclei and pavement cells (PC), which are lobed and display elongated nuclei. While guard cells have mostly 2C content, the DNA content varies between 2C and 16C in pavement cells due to one or several rounds of endoreplication and their cell size expands roughly in proportion to the amount of DNA (Melaragno et al., 1993). Epidermis cells follow the karyoplasmic ratio theory, as cell size correlates with nuclear DNA content, which increases through endoreplication (Fig. S1). A third cell type investigated was the easily accessible root hair cell (RC), which displays elongated and endoreplicated nuclei (Ketelaar et al., 2002). To assess nuclear size, shape and chromocentre organisation, nuclear DNA in whole mount

tissue was stained using the Hoechst intercalating agent (see Materials and Methods) and 3D-images of an average number of 100 nuclei for cotyledon and 40 nuclei for root hair cells were acquired from 8-10 seedlings per genotype (Table S1). 3D images of nuclei were then processed to segment the nucleus as well as the chromocentres in 3D (Fig. 1B). In order to confirm that segmented objects within the nucleus are indeed chromocentres, we simultaneously performed Hoechst DNA-staining and 3D-Fluorecence *in situ* Hybridisation (3D-FISH) on whole mount tissue. 180bp satellite repeats and 45S rDNA repeats, which are the main repetitive sequences enriched in chromosome regions forming chromocentres, were used as probes. Most of the intranuclear objects segmented using *NucleusJ* overlap with 180bp and 45S signals indicating that these are indeed chromocentres (Fig. 1C), however in certain nuclei the segmentation of chromocentres based solely on DNA stain may underestimate their exact number.

Using a dataset of 1,770 WT nuclei obtained from five biological replicates (Table S1) we computed quantitative parameters by *NucleusJ* to characterise nuclear morphology and heterochromatin organisation (Table S2). The computed parameters explain up to 60% of the phenotypic variation across the two main axes of a Principal Component Analysis (PCA) (Fig. 2A, B) and the nuclei belonging to the three different cell types form three different clouds although PC and RC are overlapping. Pavement cells display the greatest variability, root hair nuclei an intermediate variability whereas guard cell nuclei are easily grouped together (Fig. 2A). GCs exhibit nuclei of small volume (21.8±0.4 $\mu m^3$), which are rounder as indicated by reduced elongation and smoother according to a higher sphericity which take into account the volume and area of the segmented nucleus (Fig. 2C and Table S2). On the contrary, in PC and RC, the mean nuclear volumes are larger (respectively 115.2±3.4 and 123.3±3.9 $\mu m^3$) and nuclei are more elongated. The PCA analysis revealed that elongation and sphericity display a strong negative correlation ($r^2$= 0.75, P<0.0001, Fig. 2D) and are among the best parameters to discriminate the three nuclear types. In contrast, flatness, another morphological parameter only poorly discriminates the three populations of nuclei (Table S2).

Whole mount tissue preparations stained with Hoechst also gave the opportunity to correlate the nuclear shape parameters with chromocentre organisation. GC nuclei contain fewer chromocentres and a reduced total chromocentre volume per nucleus than larger nuclei such as PC and RC (Fig. 2C). We then determined a modified Relative Heterochromatin Fraction (RHF, Tessadori et al. 2007) called the Relative Heterochromatin Volume (RHV) as voxel volumes of chromocentres relative to the voxel volume of the nucleus. As we observed lower chromocentre number and volume in GC cells (Fig. 2C) and a positive correlation between the amount of heterochromatin and nuclear volume in PC (Fig. S2), we expected a constant RHV between the three cell types. However, the RHV was about two fold higher in GC compared to PC and RC due to the small

nuclear volume of the guard cells (Fig. 2C and Table S2). Finally, a strong positive correlation was observed between the number of chromocentres and the total amount of heterochromatin ($r^2$= 0.63, P<0.0001) indicating that either parameter can be used to discriminate the three cell types (Fig. 2D).

Taken together, the phenotypic variability among the three nuclear types is best explained by two nuclear shape parameters namely elongation and sphericity and the number of chromocentres.

**Chromocentres are preferentially positioned at the nuclear periphery**

Radial position, a widely used 2D parameter to characterise object position, was used to describe centromere position in living cells of various *Arabidopsis* tissues expressing HTR12 and H2B fused to fluorescent proteins (Fang and Spector, 2005). These experiments confirmed the position of chromocentres next to the nuclear periphery and the nucleolus. Furthermore, modelling also predicted that chromocentres would tend to be located at the nuclear periphery (de Nooijer et al., 2009).

Here, we took advantage of Hoechst-stained nuclei to investigate whether chromocentres preferentially localise to the nuclear periphery in the three different cell types with different nuclear shapes. To this aim, we quantified the position of each chromocentre of a given nucleus relative to the boundary of the DNA staining assuming that the intercalating agent stains the whole nuclear DNA. Three parameters were computed: (i) d(Cc border), which is the distance between the two closest voxels from the chromocentre rim and the limit of the DNA staining, (ii) d(Cc barycentre), the distance from the barycentre of each chromocentre and (iii) d(Nuc barycentre), the barycentre of the nucleus corresponding to the mass centre of the nucleus (Fig. 3A). The latter was used as a parameter to generate a theoretical uniform distribution of chromocentres for each nucleus of GC, PC and RC cells (Fig. 3B, top). When comparing to the uniform distribution of chromocentre positions, we observed that the chromocentre distances from the nuclear periphery differ from this theoretical distribution. Chromocentres are situated close to the nuclear periphery (Fig. 3B and Table S2) with mean d(Cc border) and d(Cc barycentre) parameters in GC, PC and RC of respectively 0.20±0.06, 0.30±0.11 and 0.27±0.09 µm and 0.54 ±0.09, 0.72±0.16, 0.68±0.11 µm (Fig. 3C and Table S2). The minimal distance between the chromocentres and the limit of the DNA stain (see empty rim observed in the experimental datasets, Fig.3B middle and bottom) is about 0.100 µm, which is also the resolution limit of our optical system. We therefore cannot rule out that this distance is not a biological reality, but the limit of our experimental system. Finally, the two distance parameters d(Cc border) and d(Cc barycentre) are strongly correlated in the three cell types with an overall $r^2$ of 0.85 (P<0.0001) suggesting that the three cell types share chromocentres with similar features.

Taken together the results show that chromocentres are not randomly distributed but instead

preferentially localise at a small distance from the nuclear periphery and that the distance between chromocentres and the nuclear periphery is larger in PC and RC nuclei, which show larger volumes and are less spherical.

**Alterations of nuclear shape parameters in LINC complex and lamina-like mutants**

As chromocentres are situated close to the nuclear periphery, we hypothesised that alterations of components of the LINC and lamina-like complexes might perturb position, compaction or even formation of chromocentres. Previous studies highlighted that chromatin organisation is different in distinct genetic backgrounds (Tessadori et al., 2009) and cellular contexts (Tessadori et al., 2007a); and that it depends on environmental conditions such as light (Bourbousse et al., 2015; Tessadori et al., 2007b) or growth medium (Vaillant et al., 2008). For these reasons, standardised experimental procedures were applied to reduce phenotypic variability within and across repetitions of a given genotype and mutant datasets were normalised with WT plants grown within the same experiments (Materials and Methods).

In order to evaluate the impact of mutants affecting either the LINC complex or the nuclear lamina on chromatin organisation these mutants were compared to *ddm1* and *atxr* chromatin mutants (Table 1). Loss of the chromatin remodelling factor DDM1 leads to reduced DNA methylation, altered repressive histone marks at heterochromatic regions and decondensed chromocentres (Probst et al., 2003; Soppe et al., 2000; Vongs et al., 1993). ATXR5 and ATXR6 are histone H3K27 mono-methyltransferases and the *atxr5 atxr6* double mutant displays decondensed chromocentres (Jacob et al., 2009). CRWNs are postulated to be components of the plant lamina-like structure and the *crwn1 crwn2* double mutant has previously been described to induce small nuclei (Dittmer et al., 2007) and a more condensed chromatin organisation (Grob et al., 2014; van Zanten et al., 2011; Wang et al., 2013). The quintuple *wifi* mutant (Zhou and Meier 2014), lacking three KASH proteins WIP1-3 and two WPP domain–Interacting Tail-anchored proteins WIT1-2 was selected to affect the KASH components of the LINC complex as well as some of its interactors located at the outer nuclear membrane. Finally, we combined available *sun* knockout mutant alleles in the Col-0 background (*sun1-1* (Graumann et al., 2010), *sun4-1* and *sun5-1* (Graumann et al., 2014b) to obtain double and triple mutants (Fig. S3A). The different mutant combinations of one Cter (SUN1) and two mid-SUN (SUN4 and SUN5) proteins yield viable plants, with *sun1 sun4 sun5* triple mutants showing increased leaf area compared to the WT (Fig. S3C) as well as reduced and disorganised root hair growth (Fig. S3D). Furthermore, the triple mutant most strongly affects nuclear sphericity and elongation compared to *sun1 sun4* or *sun4 sun5* double mutants (Fig. S3B) and has therefore been selected for further analysis.

We first analysed whether the 13 genes altered in our mutants (Table 1) are differentially expressed

in roots and cotyledon. For that purpose, a survey of available RNA-Seq data was performed and 8 Col-0 datasets including whole seedling roots, whole cotyledon epidermis and guard cells obtained from FACS-sorted protoplasts were selected. All genes are expressed in the different tissues although at different levels (Fig. S4). The data do not show a strong bias between cell types except for *SUN4* and *CRWN1,* which are strongly expressed respectively in epidermis and guard cells. As expected from previous work (Baubec et al., 2014), *DDM1*, *ATRX5* and *ATRX6* show weak expression in cotyledon tissue.

The different mutants were then evaluated for their impact on nuclear morphology. The 3 mutants deficient in nuclear periphery components (*wifi, sun1 sun4 sun5* and *crwn1 crwn2*) display similar profiles (Fig. 4 and Table S3). All three mutants show reduced nuclear volume, increased sphericity and decreased elongation compared to WT ($P<0.001$) the strongest effects being observed for *crwn1 crwn2*. Despite the different nuclear organisation parameters observed for the three cell types in WT plants (Fig. 2), nuclear size and form parameters are altered for all cell types in the mutants. The most prominent effects were observed in the RC cells, which are the most elongated cells in the WT, but can be seen, at the least for the sphericity parameter, also in guard cells. The two mutants with defects in chromatin organisation display a higher variability of nuclear shape parameters visible by the larger whisker plots especially for elongation in RC but the mean volume, sphericity or elongation were not significantly different from WT (Table S3).

Taken together, affecting either of the two LINC components (SUN or KASH proteins) or a component of the nuclear lamina, causes altered nuclear shapes in three different cell types with the strongest effects for the cell type with the most elongated nuclei. In contrast, mutants known to affect chromatin organisation, do not significantly impact nuclear organisation.

**Alterations of chromocentre compaction and alleviation of silencing in mutants**

Differences in heterochromatic parameters were less pronounced between WT and mutants (Fig. 5 and Table S3) except for *crwn1 crwn2,* which displays a significant reduction in the number of chromocentres in GC and RC as well as an increased RHV in all cell types (Fig. 5A, $P<0.0001$) as previously described (Dittmer et al., 2007; Grob et al., 2014; Wang et al., 2013). In *ddm1* and *atxr5 atxr6* mutants the RHV is reduced in GC and RC, but the difference is significant only in GC (Fig. 5B). When we scored the distance between the border of chromocentres and the nuclear periphery, we find that this distance is increased in all three types of nuclei in the *sun1 sun4 sun5* triple mutants (statistically significant in GC and PC, $P<0.0001$) (Fig. 5C and Table S3). Despite KASH and SUN domain proteins being part of the LINC complex (Graumann et al., 2014; Zhou and Meier, 2014), we did not detect any significant change in *wifi* mutants. This might be due to the potential redundancy with other Arabidopsis KASH domain proteins (Poulet et al., 2016) or

alternatively due to a specific function of SUN domain proteins in chromatin organisation. To correlate the differences observed in *NucleusJ* for heterochromatic parameters with the organisation of the centromeric satellite repeats, we performed 3D-FISH in whole mount preparations of cotyledons using short LNA-DNA oligonucleotide probes generated to specifically recognise the 180bp centromeric repeats (Fig. 6A and Table S4). We imaged epidermis nuclei and classed each 3D nucleus into either the condensed type (Fig. 6A, top) or the decondensed type (Fig. 6A, bottom). We noticed that at this developmental stage a significant fraction of the WT nuclei in the cotyledon epidermis are of the decondensed type (65±4%, Fig. 6B) with an equal distribution between GC and PC and that this fraction was higher in *ddm1* and *atrx5 atrx6* mutants. In the *crwn1 crwn2* double mutants that show a reduced number of chromocentres and increased chromocentre volume, these chromocentres have tendency to be more condensed than in the WT. Interestingly, while we did not detect any changes in chromocentre position in *wifi* mutants (Fig.5C), in both *wifi* and *sun1 sun4 sun5* mutant combinations, in which the LINC complex is affected, chromocentres were further decondensed compared to the WT (Fig. 6A,B). This may suggest that loss of the LINC complex affects chromocentre position and chromatin compaction through different mechanisms.

As chromatin decompaction had been correlated in certain mutants with release of transcriptional gene silencing (TGS) at centromeric and pericentromeric repeats (Jacob et al., 2009; Probst et al., 2003; Yelagandula et al., 2014), TGS release was investigated in the different mutants. Using RT-qPCR, we quantified transcript levels of the centromeric repeats 180pb (Nagaki et al., 2003) and 106B (Thompson et al., 1996) and the pericentromeric repeats called Transcriptional Silent Information (TSI) (Steimer et al., 2000) (Fig. 6C) as well as three housekeeping genes (Fig. S3). While for neither of the different mutant types, expression of the euchromatic genes was significantly altered (Fig. S3), we find as previously described (Jacob et al., 2009; Steimer et al., 2000) that TGS at TSI is alleviated in *ddm1* and *atxr5 atxr6* mutants. In agreement with the maintained chromocentre organisation in *crwn1 crwn2* mutants, centromeric and pericentromeric repeats were effectively repressed in this mutant background. In contrast, TGS in *wifi* and *sun1 sun4 sun5* was alleviated at both centromeric and pericentromeric repeats (Fig. 6C) in accordance with the increased number of nuclei with decondensed heterochromatin type.

Taken together, the organisation of centromeric repeats into chromocentres is differentially affected in mutants of the nuclear lamina or the LINC complex. Increased compaction of centromeric repeats in *crwn1 crwn2* mutants correlates with maintenance of transcriptional silencing in this mutant background. In contrast, an altered functional LINC complex causes chromocentre decondensation and affects maintenance of transcriptional gene silencing of centromeric and pericentromeric repeats.

## Discussion

In this study, we have performed in a single set of experiments a phenotypic characterisation of wild type and mutant plants affected in nuclear or heterochromatin organisation. We analysed a comprehensive dataset of more than 3,000 nuclei and scored ten 3D quantitative parameters relative to nuclear morphology and heterochromatin organisation for three distinct cell types (guard cells, pavement cells and root hair cells) in wild type and mutant backgrounds. In order to maximise the effect on nuclear morphology, we choose the quintuple *wifi* mutant (Zhou and Meier, 2014) and the triple *sun1 sun4 sun5* mutant affecting the LINC complex as well as *crwn1 crwn2* (Dittmer et al., 2007; Wang et al., 2013) affecting the potential plant lamina. Sphericity, elongation and the number of chromocentres display the best range of variations between the distinct cell types in the wild type and between wild type and mutants and therefore will provide promising phenotypic parameters to screen for new structural components of the nuclear periphery involved in nuclear morphology during interphase in the future.

The Arabidopsis nucleus is an attractive model to study the 3D position of heterochromatic repeats as these repeats cluster into chromocentre structures microscopically traceable due to their intense stain with DNA intercalating agents. A 2D parameter known as the radial distance is frequently used to compute position of chromatin domains or nuclear bodies within the nucleus (Croft et al., 1999). Radial distance defines concentric shells from the nucleus centre and while this strategy applies well for round nuclei it is less suitable for nuclei adopting ellipsoid or elongated shapes as those illustrated in Fig. 1. Furthermore, this approach requires the acquisition of 3D images, which then are projected in 2D to analyse the radial position. Here, we have opted to use spatial (3D) positioning to compute the distance and confirmed that chromocentres are located at the boundary of the Hoechst-stained nuclei in good agreement with pioneer studies using centromeric histone H3 variants (HTR12-Venus) in live cell imaging (Fang and Spector, 2005). Compared to the diploid GCs, chromocentres are situated more internally in the endoreplicated PC and RC nuclei, which also show larger volumes and a reduced heterochromatic content. The latter is in agreement with the hypothesis that endoreplicated nuclei have a more decondensed heterochromatic organisation (Schubert et al., 2012). Surprisingly, almost all of the chromocentres are close to the periphery including those usually linked to the nucleolus, which are easy to identify thanks to their larger size suggesting that the nucleolus may also localise close to the nuclear periphery in interphase nuclei.

Given the peripheral localisation of chromocentres in the different cell types, we investigated the impact of components of the LINC complex as well as the nuclear lamina on the maintenance of a repressive state at heterochromatic loci. Indeed, a current view of nuclear organisation is that chromocentres, the nucleolus and components of the nuclear lamina structure chromatin within the nuclear volume (Liu and Weigel, 2015; Simon et al., 2015). The clustering of centromeric and

pericentromeric sequences into chromocentres could compartmentalise silent chromatin away from euchromatin and thereby contribute to transcriptional repression. Furthermore, euchromatic loops are anchored at the chromocentre (Fransz et al., 2002, Grob et al., 2014) suggesting an important role for chromocentres in structuring gene rich euchromatin in nuclear space. Therefore, disorganisation of chromocentres might have more extensive impact on gene expression. The characterization of molecular components of the nuclear periphery or the inner nuclear membrane that interact with heterochromatin and chromocentres and help to anchor heterochromatin will therefore be important to better understand how the arrangement of a gene in nuclear space contributes to gene expression. While such components are to be discovered in plants, some are already described in metazoans. A well-known example is the Lamin B-receptor (LBR), a major component of the lamina, which in turn interacts with Heterochromatin Protein 1 (HP1) as well as with the methyl CpG binding protein MeCP2 (Guarda et al., 2009; Ye et al., 1997). HP1 and MeCP2 respectively recognise the repressive H3K9me2 mark and CpG DNA methylation, which are key features of heterochromatin sequences enriched in pericentromeric regions. Furthermore, lamins were also described to be associated with genomic regions known as Lamina-Associated Domains (LADs), which contain a high proportion of repeated sequences enriched in H3K27me3, a signature of facultative heterochromatin (Guelen et al., 2008; Pickersgill et al., 2006). The double *crwn1 crwn2* mutant does not decompact chromocentres nor release transcriptional silencing at heterochromatic sequences, suggesting either that the resulting imbalance of the different CRWN proteins with potentially complementary but also distinct functions results in different chromocentre structures or that different mechanisms might operate to anchor heterochromatin in plants. Indeed, neither does the plant homologue of HP1 (LHP1) localise to chromocentres nor have Lamin B-receptor homologues yet been identified in plants. However, absence of CRWN1 and CRWN2 induces chromocentre fusions. This recalls the phenotype of silent information regulator Sir4 overexpression in *Saccharomyces cerevisiae,* in which telomeric repeats are relocated from the periphery to a more central position where they cluster together. In that case, transcriptional repression increases in this new central repressive chromatin domain meaning that it can be efficiently established away from the nuclear periphery (Ruault et al., 2011).

While lamina structures are significantly divergent between metazoans and plants, the LINC complex or at least the SUN domain proteins are conserved throughout evolution (Graumann et al., 2014), suggesting that the LINC complex might play a more ancestral role in chromatin organisation. Our phenotypic analysis of the triple *sun* and *wifi* mutants revealed decompaction of chromocentres, which are located at a more internal position as well as a transcriptional derepression of heterochromatic repeats, while several euchromatic genes are expressed to similar levels as in wild type (Fig. S3). This suggests that the LINC complex affects chromatin organisation

and contributes to transcriptional repression of heterochromatic sequences. Evidence gained in *S. cerevisiae* indicated that Mps3 a Cter-SUN homologue is involved in the recruitment of heterochromatic sequences such as telomeric repeats at the nuclear envelope, an essential process needed for spindle formation in the course of chromosome segregation. This requires an indirect interaction between the N-terminal domain of Mps3 and Sir4 (Silent Information Regulator 4) or Ndj1 (Non disjunction protein 1) (Bupp et al., 2007; Conrad et al., 2007). These reports highlighting the interaction between Mps3 and telomeric repeats have been recently extended to centromeres, which also contribute to spindle formation (Fennell et al., 2015). So far, a direct interaction between chromatin and SUN proteins has only been shown for Dictyostelium SUN-1 using chromatin immunoprecipitation and Southwestern blot experiments demonstrating the capacity of the N-terminal domain of SUN-1 to bind chromatin (Xiong et al., 2008). However, the N-terminal region of Dictyostelium SUN-1 is only poorly conserved in other species including Arabidopsis (Graumann et al., 2010; Graumann et al., 2014b).

The importance of the 3D arrangement of chromatin within the nucleus and its impact on gene expression patterns is becoming an important field of investigation in animals (Tashiro and Lanctôt, 2015) and plants (Liu and Weigel, 2015). Plants perceive various stresses at the cell wall and plasma membrane, which induce reorganisation of the cytoskeleton and transmit chemical or mechanical signals to the nuclear envelope where they trigger chromatin changes affecting gene expression (Landrein and Hamant, 2013). Therefore, elucidating the mechanistic links between nuclear envelope proteins such as the LINC complex, chromatin organisation and gene expression will be an important step further for a better understanding of genome expression in response to environmental stress.

Taken together, the functional analysis of the evolutionarily conserved LINC complex strengthened evidence for its role in nuclear morphology and revealed its contribution to chromocentre positioning, heterochromatin compaction and maintenance of TGS. Further studies should be dedicated to understand whether heterochromatin alteration is a consequence of nuclear morphology alteration or intrinsic function of the LINC complex.

## Materials and methods

### Plant materials

T-DNA insertion mutants were obtained from The European Arabidopsis Stock Centre (NASC, http://arabidopsis.info/) and were all in Columbia-0 (Col-0) ecotype background. T-DNA accession numbers and genes used in this study are described in Table 1. Seed batches from all genotypes were propagated together in the greenhouse under standard conditions. After 2 days of stratification at 4ºC in the dark, *Arabidopsis* seedlings were grown under 16 h light / 8 h dark cycles at 23ºC on

germination medium containing 0.8% w/v agar, 1% w/v sucrose and 1x Murashige & Skoog salts (M0255; Duchefa Biochemie, Netherlands). Whole plants were harvested 14 days after germination (dag) for cotyledons and root observations. For each biological replicate a typical experimental plan included a WT control and one or several mutants. For each genotype, 3 plants were used for genotyping, 8-10 for 3D image analysis, 4-6 for 3D *in situ* hybridisation and 15 for RT-qPCR analysis.

**Sample preparation, Hoechst staining and 3D-FISH**

3D images were collected from cells in their original tissue environment using whole mount preparations (Bauwens et al. 1994) of 14 dag cotyledons and root hairs. Briefly, whole seedlings were collected and fixed using 1% formaldehyde, 10% DMSO in PBS 1X, EGTA 6.7mM pH7.5 under vacuum for 5 min and incubated for 25 min at room temperature. Tissues were then washed with methanol and ethanol washes to obtain transparent tissue preparations. Nuclei in whole mount preparations were either stained by Hoechst or repetitive sequences revealed by 3D-Fluorescence *in situ* Hybridization (3D-FISH) after progressive rehydration with PBS-Tween 0.1%.

For Hoechst-staining, fixed tissues were stained overnight at 4°C in a solution of Hoechst 33258 (SIGMA) at 25µg/ml in PBS. To perform live cell imaging, DNA was stained using PicoGreen® (Molecular probes) diluted to 1/400 in 0.01% Triton-X100 for 1 hour at room temperature.

Samples were then washed three times with PBS 1X, excess water removed with paper tissue and placed on a slide in PBS/glycerol (20:80) solution and covered with a cover slip for microscopic observations. For 3D-FISH, hydrated tissues were washed twice in 2xSSC then incubated for 30 min in 2xSSC:HB50 (1:1) (50% formamide, 2xSSC, 50 mM sodium phosphate pH7) and finally 30 min in HB50. Tissues were directly immersed in HB50 containing 1µM final of Locked Nucleic Acid (LNA) probes specific for the 180bp centromeric repeats (Exiqon; GTATGATTGAGTATAAGAACTTAAACC). Tissues were hybridised overnight at 37°C, rinsed twice for 30 min at 42°C in SF50 (50% formamide, 2xSSC) and incubated overnight with 0.25µg/ml Hoechst 33258 in PBS at 4°C. Samples were rinsed twice in 2xSSC and twice in PBS and mounted in PBS:glycerol (20:80) as described above.

To reveal simultaneously the 45S rDNA loci and the centromeric 180bp repeats, the probes were labelled with Cy3-dUTP or Cy5-dUTP (GE healthcare) by nick-translation (Roche) using a plasmid containing the 45S rDNA sequence from *Triticum aestivum* (Gerlach and Bedbrook, 1979) or the 180bp probe from *Arabidopsis thaliana* (Martinez-Zapater et al., 1986) and 3D FISH experiments were performed as previously (Bauwens et al., 1994).

**Microscope and 3D imaging methods**

Microscopic observations were performed by structured illumination microscopy to produce confocal-like images using an Optigrid module (Leica-microsystems MAAF DM 16000B). All images were acquired using a 63x oil objective allowing a theoretical resolution of xy = 0.24 and z = 0.46 µm further reduced by the factor 2.3 according to the Nyquist-Shannon sampling theorem (Pawley, 2006) such that the final lateral and axial resolution used in this study were respectively xy = 0.1 and z = 0.2 µm. Furthermore, all initial anisotropic voxels are converted to isotropic voxel (i.e. cubic, xyz = 0.1 µm) prior to calculation (Poulet et al., 2015). The *ImageJ* plugin *NucleusJ* was used to characterise nuclear morphology and chromatin organisation (Poulet et al., 2015). A detailed description of the quantitative parameters generated by *NucleusJ* can be found in supplemental materials of Poulet et al. (2015). d(Nuc barycentre) is the barycentre of the nucleus measured by computing the distance map of the nucleus, which is the distance between each voxel of a given nucleus and the limit of the image background. Computation of the distance map is realised with the ImageJ plugin developed by Bob Dougherty (http://www.optinav.com/download/LocalThickness .jar) and is based on the Euclidean distance transformation (Saito and Toriwaki, 1994). d(Nuc barycentre) has been preferred to the Equivalent Spherical Radius (ESR) generated by NucleusJ as most of the nuclei investigated in this study are not spherical but instead have elongated morphology. Theoretical data for the chromocentre distance for each nucleus were generated using the R package *runif* function to produce a theoretical uniform distribution on the interval from *min* (min = 0 at the nuclear periphery) to *max* (max = barycentre of the nucleus). The number *n* of chromocentres visualized as points per nucleus equals the number of chromocentres detected for each nucleus.

**RNA extraction and RT-qPCR**

Total RNAs were extracted from 30 cotyledons using Tri-Reagent (Euromedex), treated with RQ1 DNase I (Promega) and purified using phenol-chloroform extraction. Reverse transcription was primed either with oligo(dT)15 or with random hexamers using M-MLV reverse transcriptase (Promega) (Table S4). The resulting cDNAs were diluted three times and further used in quantitative PCR with the LightCycler® 480 SYBR Green I Master kit on the Roche LightCycler® 480. Transcript levels of interest were normalised to *SAND* (At2g28390) (Czechowski et al., 2005) using the comparative threshold cycle method.

**Statistics**

Statistical analyses were performed using R (The R Core Team, 2015). All boxplots are represented as box containing 50% of the individuals starting from the first quartile (Q1) to the third quartile (Q3) with whiskers equal to 1.5 of the interquartile range (IQR = Q1-Q3). Principal component

analysis (PCA) was carried out with the FactoMineR package, an extension of R (Lê et al., 2008). R scripts were developed to automatically undertake statistical tests (t-test and correlation), generate PCA and boxplots on the data obtained after 3D image analysis using *NucleusJ*. A Student's t-test was used to compare the theoretical uniform distribution of chromocentres to the observed data (distance chromocentre border to nuclear border and distance chromocentre barycentre to nuclear border) and means between wild type and mutant backgrounds for RT-qPCR. A proportion test was applied to analyse the significance of the proportion of condensed chromocentres.

**Acknowledgments**

We thank Iris Meier (Ohio State University, USA) for providing *wifi* seeds and information about *WIP* and *WIT* genes and mutants, Paul Fransz (University of Amsterdam, NL) for technical advice and training in 3D-FISH experiments and Maxime Claux for technical assistance in graphical representations.

**Competing interests:** The authors declare no competing interests.

**Author contributions:** A.V.P. and C.T. supervised the study. A.P., S.D., C.D. and M. V. performed experiments. A.P. and C.T. designed the study and analysed the data. A.V.P., D.E.E and C.T. wrote the manuscript.

**Funding**

This work was supported by Auvergne and Oxford Brookes universities to AP, by the French National Research Agency (ANR-11 JSV2 009 01, ANR-12-ISV6-0001 to AVP), by the Region Auvergne and FEDER (Life GRID to CT) and Centre National de la Recherche Scientifique (PEPS-site to CT).

**REFERENCES**

**Adams, R. L. and Wente, S. R.** (2013). Uncovering Nuclear Pore Complexity with Innovation. *Cell* **152**, 1218–1221.

**Anders, S., Pyl, P. T. and Huber, W.** (2015). HTSeq–a Python framework to work with high-throughput sequencing data. *Bioinformatics* **31**, 166–169.

**Baubec, T., Finke, A., Mittelsten Scheid, O. and Pecinka, A.** (2014). Meristem-specific expression of epigenetic regulators safeguards transposon silencing in Arabidopsis. *EMBO Rep.* **15**, 446–452.

**Bauwens, S., Katsanis, K., Van Montagu, M., Van Oostveldt P., and Engler G.** (1994).

Procedure for Whole Mount Fluorescence in Situ Hybridization of Interphase Nuclei on *Arabidopsis thaliana*. *The Plant Journal* **6**: 123–131.

**Bickmore, W. A. and van Steensel, B.** (2013). Genome Architecture: Domain Organization of Interphase Chromosomes. *Cell* **152**, 1270–1284.

**Bourbousse, C., Mestiri, I., Zabulon, G., Bourge, M., Formiggini, F., Koini, M. A., Brown, S. C., Fransz, P., Bowler, C. and Barneche, F.** (2015). Light signaling controls nuclear architecture reorganization during seedling establishment. *Proc. Natl. Acad. Sci. U. S. A.* **112**, 2836–2844.

**Bourdon, M., Pirrello, J., Cheniclet, C., Coriton, O., Bourge, M., Brown, S., Moïse, A., Peypelut, M., Rouyère, V., Renaudin, J.-P., et al.** (2012). Evidence for karyoplasmic homeostasis during endoreduplication and a ploidy-dependent increase in gene transcription during tomato fruit growth. *Development* **139**, 3817–3826.

**Bupp, J. M., Martin, A. E., Stensrud, E. S. and Jaspersen, S. L.** (2007). Telomere anchoring at the nuclear periphery requires the budding yeast Sad1-UNC-84 domain protein Mps3. *J. Cell Biol.* **179**, 845–854.

**Cavalier-Smith, Thomas** (2005). Economy, Speed and Size Matter: Evolutionary Forces Driving Nuclear Genome Miniaturization and Expansion. *Annals of Botany* **95**, 147 –175.

**Conrad, M. N., Lee, C.-Y., Wilkerson, J. L. and Dresser, M. E.** (2007). MPS3 mediates meiotic bouquet formation in Saccharomyces cerevisiae. *Proc. Natl. Acad. Sci. U. S. A.* **104**, 8863–8868.

**Crisp, Melissa, Liu, Q., Roux, K., Rattner, J. B., Shanahan, C., Burke, B., Stahl, P. D. and Hodzic D.** (2006). Coupling of the Nucleus and Cytoplasm Role of the LINC Complex. *The Journal of Cell Biology* **172**, 41–53.

**Croft, J. A., Bridger, J. M., Boyle, S., Perry, P., Teague, P. and Bickmore, W. A.** (1999). Differences in the Localization and Morphology of Chromosomes in the Human Nucleus. *J. Cell Biol.* **145**, 1119–1131.

**Czechowski, T., Stitt, M., Altmann, T., Udvardi, M. K. and Scheible, W.-R.** (2005). Genome-Wide Identification and Testing of Superior Reference Genes for Transcript Normalization in Arabidopsis. *Plant Physiol.* **139**, 5–17.

**de Nooijer, S., Wellink, J., Mulder, B. and Bisseling, T.** (2009). Non-specific interactions are sufficient to explain the position of heterochromatic chromocenters and nucleoli in interphase nuclei. *Nucleic Acids Res.* **37**, 3558–3568.

**Dittmer, Travis A., Stacey, N. J., Sugimoto-Shirasu, K. and Richards, E. J**. (2007). LITTLE NUCLEI Genes Affecting Nuclear Morphology in *Arabidopsis thaliana*. *The Plant Cell* **19**, 2793–2803.

**Fang, Y. and Spector, D. L.** (2005). Centromere positioning and dynamics in living Arabidopsis plants. *Mol. Biol. Cell* **16**, 5710–5718.

**Feng, C.-M., Qiu, Y., Van Buskirk, E. K., Yang, E. J. and Chen, M.** (2014). Light-regulated gene repositioning in Arabidopsis. *Nat. Commun.* **5**, 3027–3038.

**Fennell, A., Fernández-Álvarez, A., Tomita, K. and Cooper, J. P.** (2015). Telomeres and centromeres have interchangeable roles in promoting meiotic spindle formation. *J. Cell Biol.* **208**,

415–428.

**Fransz, P., De Jong, J. H., Lysak, M., Castiglione, M. R. and Schubert, I.** (2002). Interphase chromosomes in Arabidopsis are organized as well defined chromocenters from which euchromatin loops emanate. *Proc. Natl. Acad. Sci. U. S. A.* **99**, 14584–14589.

**Gerlach, W. L. and Bedbrook, J. R.** (1979). Cloning and characterization of ribosomal RNA genes from wheat and barley. *Nucleic Acids Res.* **7**, 1869–1885.

**Gerlitz, G. and Bustin, M.** (2011). The role of chromatin structure in cell migration. *Trends Cell Biol.* **21**, 6–11.

**Goehring, N. W. and Hyman, A. A.** (2012). Organelle Growth Control through Limiting Pools of Cytoplasmic Components. *Curr. Biol.* **22**, 330–339.

**Goto, C., Tamura, K., Fukao, Y., Shimada, T. and Hara-Nishimura, I.** (2014a). The Novel Nuclear Envelope Protein KAKU4 Modulates Nuclear Morphology in Arabidopsis. *Plant Cell* **26**, 2143–2155.

**Goto, C., Tamura, K., Fukao, Y., Shimada, T. and Hara-Nishimura, I.** (2014b). The Novel Nuclear Envelope Protein KAKU4 Modulates Nuclear Morphology in Arabidopsis. *Plant Cell Online* **26**, 2143-2155.

**Graumann, K., Evans D. E.** (2010). The Plant Nuclear Envelope in Focus. *Biochemical Society Transactions* **38**, 307–311.

**Graumann, K., Evans D. E.** (2013). The Nuclear Envelope - Structure and Protein Interactions. *Annual Plant Reviews* **46**, 19–56.

**Graumann, K., Runions, J. and Evans, D. E.** (2010). Characterization of SUN□domain proteins at the higher plant nuclear envelope. *Plant J.* **61**, 134–144.

**Graumann, K., Vanrobays, E., Tutois, S., Probst, A. V., Evans, D. E. and Tatout, C.** (2014). Characterization of two distinct subfamilies of SUN-domain proteins in Arabidopsis and their interactions with the novel KASH-domain protein AtTIK. *J. Exp. Bot.* **65**, 6499–6512.

**Grob, S., Schmid, M. W. and Grossniklaus, U.** (2014). Hi-C Analysis in Arabidopsis Identifies the KNOT, a Structure with Similarities to the flamenco Locus of Drosophila. *Mol. Cell* **55**, 678–693.

**Guarda, A., Bolognese, F., Bonapace, I. M. and Badaracco, G.** (2009). Interaction between the inner nuclear membrane lamin B receptor and the heterochromatic methyl binding protein, MeCP2. *Exp. Cell Res.* **315**, 1895–1903.

**Guelen, L., Pagie, L., Brasset, E., Meuleman, W., Faza, M. B., Talhout, W., Eussen, B. H., de Klein, A., Wessels, L., de Laat, W., et al.** (2008). Domain organization of human chromosomes revealed by mapping of nuclear lamina interactions. *Nature* **453**, 948–951.

**Jacob, Y., Feng, S., LeBlanc, C. A., Bernatavichute, Y. V., Stroud, H., Cokus, S., Johnson, L. M., Pellegrini, M., Jacobsen, S. E. and Michaels, S. D.** (2009). ATXR5 and ATXR6 are H3K27 monomethyltransferases required for chromatin structure and gene silencing. *Nat. Struct. Mol. Biol.* **16**, 763–768.

**Janski, N., Masoud, K., Batzenschlager, M., Herzog, E., Evrard, J.-L., Houlné, G., Bourge, M., Chabouté, M.-E. and Schmit, A.-C.** (2012). The GCP3-Interacting Proteins GIP1 and GIP2 Are Required for γ-Tubulin Complex Protein Localization, Spindle Integrity, and Chromosomal Stability. *The Plant Cell Online* **24**, 1171–1187.

**Jordan, N. D., West, J. P., Bottley, A., Sheikh, M. and Furner, I.** (2007). Transcript profiling of the hypomethylated hog1 mutant of Arabidopsis. *Plant Mol. Biol.* **65**, 571–586.

**Jovtchev, G., Schubert V., Meister A., Barow M., and Schubert I.** (2006). Nuclear DNA Content and Nuclear and Cell Volume Are Positively Correlated in Angiosperms. *Cytogenetic and Genome Research* **114**, 77–82.

**Ketelaar, T., Faivre-Moskalenko, C., Esseling, J. J., Ruijter, N. C. A. de, Grierson, C. S., Dogterom, M. and Emons, A. M. C.** (2002). Positioning of Nuclei in Arabidopsis Root Hairs An Actin-Regulated Process of Tip Growth. *Plant Cell* **14**, 2941–2955.

**Kim, D., Pertea, G., Trapnell, C., Pimentel, H., Kelley, R., Salzberg, S. L. and others** (2013). TopHat2: accurate alignment of transcriptomes in the presence of insertions, deletions and gene fusions. *Genome Biol* **14**, R36.

**Landrein, B. and Hamant, O.** (2013). How mechanical stress controls microtubule behavior and morphogenesis in plants: history, experiments and revisited theories. *Plant J.* **75**, 324–338.

**Lê, S., Josse, J., Husson, F. and others** (2008). FactoMineR: an R package for multivariate analysis. *J. Stat. Softw.* **25**, 1–18.

**Levy, D. L. and Heald, R.** (2010). Nuclear Size Is Regulated by Importin α and Ntf2 in Xenopus. *Cell* **143**, 288–298.

**Liu, C. and Weigel, D.** (2015). Chromatin in 3D: progress and prospects for plants. *Genome Biol.* **16**, 170.

**Martinez-Zapater, J. M., Estelle, M. A. and Somerville, C. R.** (1986). A highly repeated DNA sequence in *Arabidopsis thaliana*. *Mol. Gen. Genet. MGG* **204**, 417–423.

**Mattout, A., Cabianca, D. S. and Gasser, S. M.** (2015). Chromatin states and nuclear organization in development — a view from the nuclear lamina. *Genome Biol.* **16**, 174–189.

**Méjat, A. and Misteli, T.** (2010). LINC complexes in health and disease. *Nucleus* **1**, 40–52.

**Melaragno, J. E., Mehrotra, B., Coleman, A. W**. (1993). Relationship Between Endopolyploidy and Cell Size in Epidermal Tissue of Arabidopsis. *The Plant Cell Online* **5**: 1661–1668.

**Nagaki, K., Talbert, P. B., Zhong, C. X., Dawe, R. K., Henikoff, S. and Jiang, J.** (2003). Chromatin Immunoprecipitation Reveals That the 180-bp Satellite Repeat Is the Key Functional DNA Element of Arabidopsis thaliana Centromeres. *Genetics* **163**, 1221–1225.

**Neumann, F. R. and Nurse, P.** (2007). Nuclear size control in fission yeast. *J. Cell Biol.* **179**, 593–600.

**Oda, Y., Fukuda, H.** (2011). Dynamics of Arabidopsis SUN Proteins During Mitosis and Their Involvement in Nuclear Shaping. *The Plant Journal* **66**, 629–641.

**Pawley, J. B.** (2006). Points, Pixels, and Gray levels: Digitizing Image Data. In *Handbook of*

*Biological Confocal Microscopy* (ed. James B. Pawley), pp59-79. Springer

**Pickersgill, H., Kalverda, B., de Wit, E., Talhout, W., Fornerod, M. and van Steensel, B.** (2006). Characterization of the Drosophila melanogaster genome at the nuclear lamina. *Nat. Genet.* **38**, 1005–1014.

**Poulet, A., Arganda-Carreras, I., Legland, D., Probst, A. V., Andrey, P. and Tatout, C.** (2015). NucleusJ: an ImageJ plugin for quantifying 3D images of interphase nuclei. *Bioinformatics* **31**, 1144–1146.

**Poulet, A., Probst, A. V., Graumann, K., Tatout, C. and Evans, D.** (2016). Exploring the evolution of the proteins of the plant nuclear envelope. *Nucleus*: 1–14. [Epub ahead of print]

**Probst, A. V., Fransz, P. F., Paszkowski, J. and Mittelsten Scheid, O.** (2003). Two means of transcriptional reactivation within heterochromatin. *Plant J. Cell Mol. Biol.* **33**, 743–749.

**Qian, P., Hou, S. and Guo, G.** (2009). Molecular mechanisms controlling pavement cell shape in Arabidopsis leaves. *Plant Cell Rep.* **28**, 1147–1157.

**Ruault, M., De Meyer, A., Loïodice, I. and Taddei, A.** (2011). Clustering heterochromatin: Sir3 promotes telomere clustering independently of silencing in yeast. *J. Cell Biol.* **192**, 417–431.

**Saito, T. and Toriwaki, J.-I.** (1994). New algorithms for euclidean distance transformation of an n-dimensional digitized picture with applications. *Pattern Recognition*, **27**:1551-1565.

**Schubert, V., Berr, A. and Meister, A.** (2012). Interphase chromatin organisation in Arabidopsis nuclei: constraints versus randomness. *Chromosoma* **121**, 369–87.

**Shumaker, D. K., Dechat, T., Kohlmaier, A., Adam, S. A., Bozovsky, M. R., Erdos, M. R., Eriksson, M., Goldman, A. E., Khuon, S., Collins, F. S., et al.** (2006). Mutant nuclear lamin A leads to progressive alterations of epigenetic control in premature aging. *Proc. Natl. Acad. Sci. U. S. A.* **103**, 8703–8708.

**Simon, L., Voisin, M., Tatout, C. and Probst, A. V.** (2015). Structure and Function of Centromeric and Pericentromeric Heterochromatin in *Arabidopsis thaliana*. *Front Plant Sci.* **30**, 1049–1057.

**Soppe, W. J. ., Jacobsen, S. E., Alonso-Blanco, C., Jackson, J. P., Kakutani, T., Koornneef, M. and Peeters, A. J. .** (2000). The Late Flowering Phenotype of fwa Mutants Is Caused by Gain-of-Function Epigenetic Alleles of a Homeodomain Gene. *Mol. Cell* **6**, 791–802.

**Steimer, A., Amedeo, P., Afsar, K., Fransz, P., Scheid, O. M. and Paszkowski, J.** (2000). Endogenous Targets of Transcriptional Gene Silencing in Arabidopsis. *Plant Cell Online* **12**, 1165–1178.

**Sugimoto-Shirasu, K., Roberts, G. R., Stacey, N. J., McCann, M. C., Maxwell, A. and Roberts, K.** (2005). RHL1 Is an Essential Component of the Plant DNA Topoisomerase VI Complex and Is Required for Ploidy-dependent Cell Growth. *Proc. Natl. Acad. Sci. U. S. A.* **102**, 18736–18741.

**Sugimoto-Shirasu, K. and Roberts, K.** (2003). "Big it up": endoreduplication and cell-size control in plants. *Curr. Opin. Plant Biol.* **6**, 544–553.

**Tamura, K., and Hara-Nishimura, I.** (2011). Involvement of the Nuclear Pore Complex in Morphology of the Plant Nucleus. *Nucleus* **2**, 168–172.

**Tamura, K., Fukao, Y., Iwamoto, M., Haraguchi, T. and Hara-Nishimura, I**. (2010). Identification and Characterization of Nuclear Pore Complex Components in *Arabidopsis thaliana*. *The Plant Cell Online* **22**, 4084–4097.

**Tashiro, S. and Lanctôt, C.** (2015). The International Nucleome Consortium. *Nucleus* **6**, 89–92.

**Tessadori, F., Chupeau, M.-C., Chupeau, Y., Knip, M., Germann, S., van Driel, R., Fransz, P. and Gaudin, V.** (2007a). Large-scale dissociation and sequential reassembly of pericentric heterochromatin in dedifferentiated Arabidopsis cells. *J. Cell Sci.* **120**, 1200–1208.

**Tessadori, F., Schulkes, R. K., Driel, R. van and Fransz, P.** (2007b). Light□regulated large□scale reorganization of chromatin during the floral transition in Arabidopsis. *Plant J.* **50**, 848–857.

**Tessadori, F., van Zanten, M., Pavlova, P., Clifton, R., Pontvianne, F., Snoek, L. B., Millenaar, F. F., Schulkes, R. K., van Driel, R., Voesenek, L. A. C. J., et al.** (2009). Phytochrome B and histone deacetylase 6 control light-induced chromatin compaction in *Arabidopsis thaliana*. *PLoS Genet.* **5**, e1000638.

**The R Core Team** (2015). R: A Language and Environment for Statistical Computing. *R Foundation for Statistical Computing* **Version 3.2.3**.

**Thompson, H. L., Schmidt, R. and Dean, C.** (1996). Identification and distribution of seven classes of middle-repetitive DNA in the *Arabidopsis thaliana* genome. *Nucleic Acids Res.* **24**, 3017–3022.

**Traas, J., Hülskamp, M., Gendreau, E. and Höfte, H. (**1998). Endoreduplication and Development: Rule Without Dividing? *Current Opinion in Plant Biology* **1**, 498–503.

**Vaillant, I., Tutois, S., Jasencakova, Z., Douet, J., Schubert, I. and Tourmente, S.** (2008). Hypomethylation and hypermethylation of the tandem repetitive 5S rRNA genes in Arabidopsis. *Plant J. Cell Mol. Biol.* **54**, 299–309.

**Van Zanten, M., Koini, M. A., Geyer, R., Liu, Y., Brambilla, V., Bartels, D., Koornneef, M., Fransz, P. and Soppe, Wim J. J.** (2011). Seed maturation in *Arabidopsis thaliana* is characterized by nuclear size reduction and increased chromatin condensation. *Proc. Natl. Acad. Sci. U. S. A.* **108**, 20219–20224.

**Vongs, A., Kakutani, T., Martienssen, R. A. and Richards, E. J.** (1993). *Arabidopsis thaliana* DNA methylation mutants. *Science* **260**, 1926–1928.

**Wang, H., Dittmer, T. A. and Richards, E. J.** (2013). Arabidopsis CROWDED NUCLEI (CRWN) proteins are required for nuclear size control and heterochromatin organization. *BMC Plant Biol.* **13**, 200.

**Webster, M., Witkin, K. L. and Cohen-Fix, O.** (2009). Sizing up the nucleus: nuclear shape, size and nuclear-envelope assembly. *J. Cell Sci.* **122**, 1477–1486.

**Xiong, H., Rivero, F., Euteneuer, U., Mondal, S., Mana-Capelli, S., Larochelle, D., Vogel, A., Gassen, B. and Noegel, A. A.** (2008). Dictyostelium Sun-1 Connects the Centrosome to Chromatin and Ensures Genome Stability. *Traffic* **9**, 708–724.

**Ye, Q., Callebaut, I., Pezhman, A., Courvalin, J.-C. and Worman, H. J.** (1997). Domain-specific

Interactions of Human HP1-type Chromodomain Proteins and Inner Nuclear Membrane Protein LBR. *J. Biol. Chem.* **272**, 14983–14989.

**Yelagandula, R., Stroud, H., Holec, S., Zhou, K., Feng, S., Zhong, X., Muthurajan, U. M., Nie, X., Kawashima, T., Groth, M., et al.** (2014). The Histone Variant H2A.W Defines Heterochromatin and Promotes Chromatin Condensation in Arabidopsis. *Cell* **158**, 98–109.

**Zhou, X. and Meier, I.** (2014). Efficient plant male fertility depends on vegetative nuclear movement mediated by two families of plant outer nuclear membrane proteins. *Proc. Natl. Acad. Sci. U. S. A.* **111**, 11900–11905.

**Zhou, X., Graumann, K., Evans, D. E., and Meier, I.** (2012). Novel Plant SUN–KASH Bridges Are Involved in RanGAP Anchoring and Nuclear Shape Determination. *The Journal of Cell Biology* **196**, 203–211.

**Zhou, X., Graumann, K. and Meier, I.** (2015a). The plant nuclear envelope as a multifunctional platform LINCed by SUN and KASH. *J. Exp. Bot.* **66**, 1649–1659.

**Zhou, X., Groves, N. R. and Meier, I.** (2015b). Plant nuclear shape is independently determined by the SUN-WIP-WIT2-myosin XI-i complex and CRWN1. *Nucleus* **6**, 144–153.

## Table

**Table 1: Mutants used in this study**

Mutant description can be found in Zhou and Meier (2014) for *wifi*, Dittmer *et al.* (2007) for *crwn1 crwn2*, and Jacobs *et al.* (2009) for *atxr5 atxr6*. To keep working in Col-0 genetic background, the *ddm1-10* T-DNA insertion was selected in this work (Jordan et al., 2007). The *sun1 sun4 sun5* triple mutant has been generated for the first time in this study and is described in Figure S1.

| Mutant names | Alleles | T-DNA | Gene Name | Acc Number | Family | Mutant class |
|---|---|---|---|---|---|---|
| ***wifi*** | *wit1-1* | GABI-Kat 470E06 | *WIT1* | At5g11390 | KASH-interacting | Nuclear periphery |
| | *wit2-1* | SALK_CS39986 | *WIT2* | At1g68910 | | |
| | *wip1-1* | SAIL_390_A08 | *WIP1* | At4g26455 | KASH | |
| | *wip2-1* | SALK_052226 | *WIP2* | At5g56210 | | |
| | *wip3-1* | GABI-Kat 459H07 | *WIP3* | At3g13360 | | |
| ***sun1 sun4 sun5*** | *sun1-1* | SAIL_84_G10 | *SUN1* | At5g04990 | SUN | |
| | *sun4-1* | SALK_022028 | *SUN4* | At1g71360 | | |
| | *sun5-1* | SALK_126070C | *SUN5* | At4g23950 | | |
| ***crwn1 crwn2*** | *crwn1-1* | SALK_023383 | *CRWN1* | At1g67230 | Lamin-like | |
| | *crwn2-1* | SALK_090952 | *CRWN2* | At1g13220 | | |
| ***ddm1*** | *ddm1-10* | SALK_000590 | *DDM1* | At5g66750 | Chromatin remodeller | Chromatin |
| ***atxr5 atxr6*** | *atxr5-1* | SALK_130607C | *ATXR5* | At5g09790 | Histone methyl transferase | |
| | *atxr6-1* | SAIL_240_H01 | *ATXR6* | At5g24340 | | |

## Figures

**Fig. 1: 3D segmentation of nuclei and chromocentres using *NucleusJ***

**A)** Maximum Z projections of guard cells (GC), pavement cells (PC) and root hair cell (RC) nuclei stained with Hoechst DNA intercalating-agent. Chromocentres correspond to bright nuclear foci. **B)** Same nuclei as in A) subjected to *NucleusJ* 3D segmentation to delimit the nucleus and the chromocentres. Results of nucleus and chromocentre segmentation are shown as an overlay of the maximal Z projection of nucleus (blue) and chromocentres (pink). **C)** 3D-FISH experiments. Images of maximal Z projections of a PC nucleus stained with Hoechst processed by *NucleusJ* to obtain the segmented nucleus (blue) and chromocentres (Cc, pink) as well as the 45SrDNA (red) and centromeric 180bp satellite repeats (green) signals. Scale bar = 2µm.

**Fig. 2: Phenotypic variability of guard cell, pavement cell and root hair cell nuclei in wild type plants can be explained by several 3D nuclear parameters**

Principal component analysis of **A)** individual nuclei from guard cells (GC, n=697, black), pavement cells (PC, n=590, green) and root hair cells (RC, n=213, red) and **B)** quantitative parameters generated by *NucleusJ* are depicted in two main axes. Nuclear volume (Volume), total volume of all chromocentres (VCcTotal), number of chromocentres (NbCc). **C)** Selected *NucleusJ* parameters highlight the phenotypic variations among the three types of nuclei. Complete analysis is given in Table S2. **D)** Scatter plot matrix and absolute correlation between pairs of variables. The two major correlations between elongation and sphericity ($r^2$=0.75) and NbCc and VCcTotal ($r^2$=0.63) are highlighted in yellow and orange respectively. *: P≤0.01, **:P≤0.001, ***: P≤0.0001.

**Fig. 3: Chromocentres are located close to the nuclear periphery**

**A)** *NucleusJ* computes the distance between the limit of the Hoechst DNA-staining (blue) and the chromocentres (Cc, pink) boundary (d(Cc border)) or barycentre (d(Cc barycentre)). The barycentre of the nucleus d(Nuc barycentre) (white cross) is also indicated. **B)** Graphical representation of chromocentre distribution in respect to the limit of Hoechst DNA-staining among the three cell types. Theoretical uniform distribution of chromocentres (top) is compared to observed distributions for d(Cc border) (middle) and d(Cc barycentre) (bottom). The uniform distribution of chromocentres is obtained by placing the same number of chromocenters as in the corresponding datasets between the periphery and the corresponding nuclear barycentres, for each nucleus of the dataset. Chromocentres and nuclei numbers are given at the bottom of the figure. The scales of the graphs were standardized setting the maximum d(Nuc barycentre**)** value at 2.5 µm to include all the data in the graphical representations. A Student t-test has been used to demonstrate the non-random distribution of chromocentres in the six observed datasets ($P<2.2\ 10^{-16}$). **C)** Boxplots of d(Cc

555 border) and d(Cc barycentres) in the three observed datasets. Statistical differences determined using a
556 Kruskal-Wallis non-parametric test are indicated above box-plots. GC: guard cells (black), PC:
557 pavement cells (green), RC: root hair cells (red). *: P≤0.01, **:P≤0.001, ***: P≤0.0001 and ns: not
558 significant.
559
560 **Fig. 4: Alteration of nuclear morphology in mutant nuclei from guard cells, pavement cells**
561 **and root hair cells.**
562 Tukey boxplots of nuclear morphology parameters highlighting the phenotypic variations in three
563 types of nuclei (GC in gray, PC in green and RC in red) for five mutant backgrounds. All
564 parameters recorded for mutant backgrounds were standardised using WT mean set as 1 (red dashed
565 line). *: P≤0.001. Number of analysed nuclei and a more detailed statistical analysis are available
566 respectively in Table S1 and S3.
567
568 **Fig. 5: Alteration of chromatin organisation in mutant nuclei from guard cells, pavement cells**
569 **and root hair cells.**
570 Tukey boxplots of chromatin organisation parameters highlighting the phenotypic variations in
571 three types of nuclei (GC in gray, PC in green and RC in red) for five mutant backgrounds. All
572 parameters recorded for mutant backgrounds were standardised using WT mean set as 1 (red dashed
573 line). *: P≤0.001. Number of analysed nuclei and a more detailed statistical analysis are available
574 respectively in Table S1 and S3.
575
576 **Fig. 6: Alleviation of transcriptional repression of heterochromatic repeat sequences in LINC**
577 **mutants**
578 **A)** Representative nuclei shown as maximal Z projection collected from 3D-FISH experiments on
579 nuclei counterstained with DAPI (blue) of cotyledon epidermis using a fluorescent probe against
580 180bp satellite repeats (red). **B)** Quantification of condensed and decondensed 180bp hybridisation
581 signals recorded by 3D-FISH obtained from 4 independent cotyledons. Average ± SEM. Number of
582 nuclei ranging from n =27 to 56 are available in Table S5. **C)** Transcription level of TSI, 180bp and
583 106B scored by RT-qPCR. Histograms show means of transcript levels ± SEM obtained for two
584 independent PCR amplifications of three biological replicates. The y-axis shows the fold change
585 relative to WT (set to 1) after normalisation to expression of At2g28390 (*SAND*). *: P≤0.05.

# Figure 1

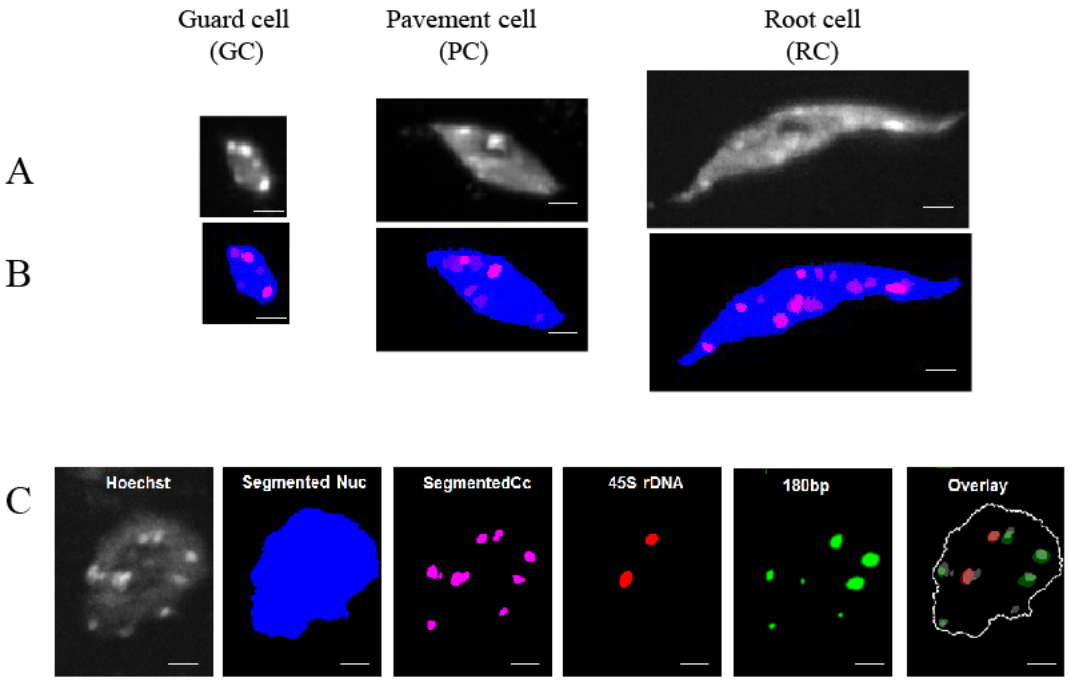
Guard cell
(GC)
Pavement cell
(PC)
Root cell
(RC)
A
B
C
Hoechst
Segmented Nuc
SegmentedCc
45S rDNA
180bp
Overlay

586

# Figure 2

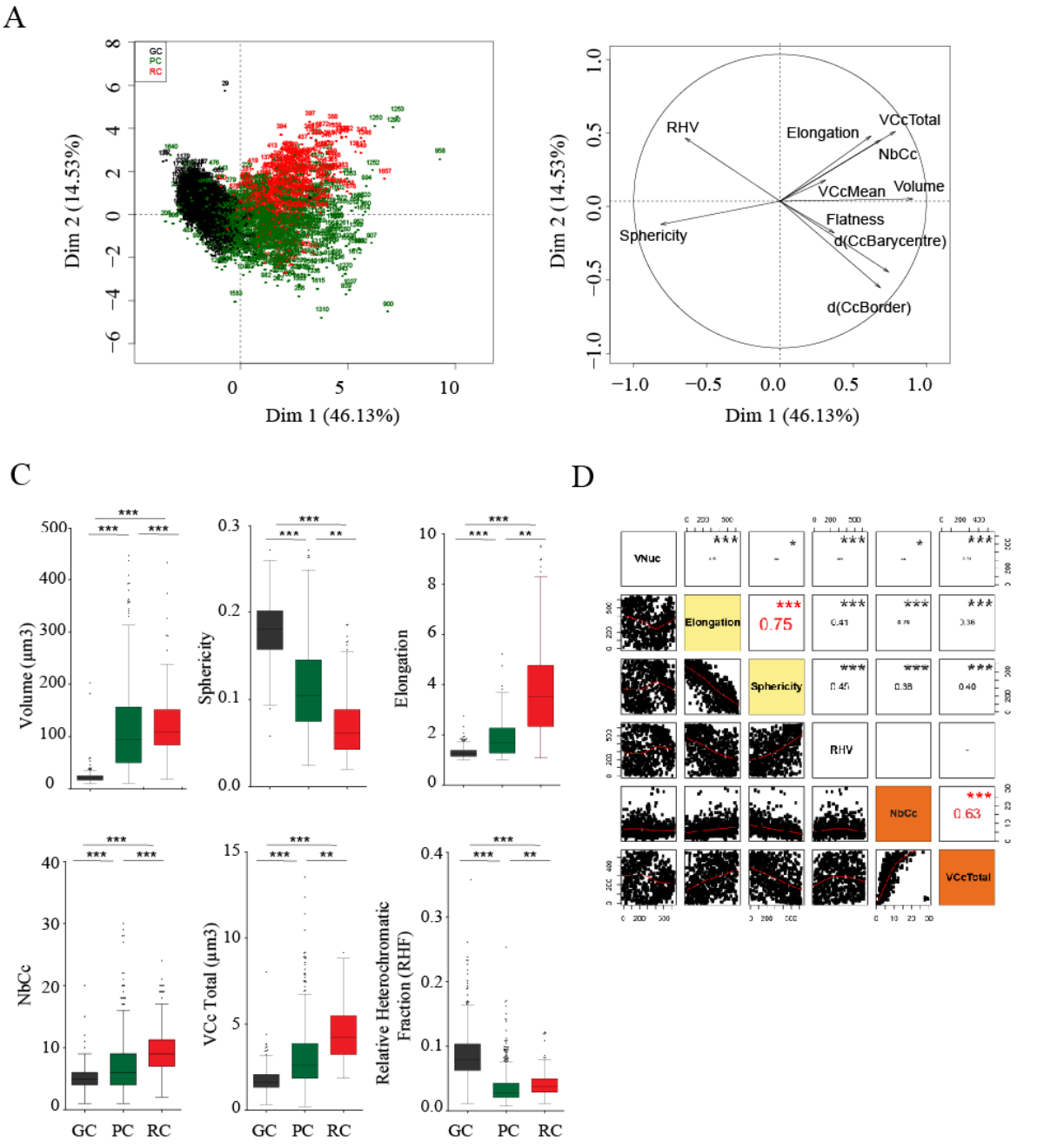
A
GC
PC
RC
Dim 2 (14.53%)
Dim 1 (46.13%)
RHV
Elongation
VCcTotal
NbCc
VCcMean
Volume
Flatness
Sphericity
d(CcBarycentre)
d(CcBorder)
C
Volume (µm3)
Sphericity
Elongation
NbCc
VCc Total (µm3)
Relative Heterochromatic Fraction (RHF)
D
VNuc
Elongation
0.75
Sphericity
RHV
NbCc
0.63
VCcTotal

587

Figure 3

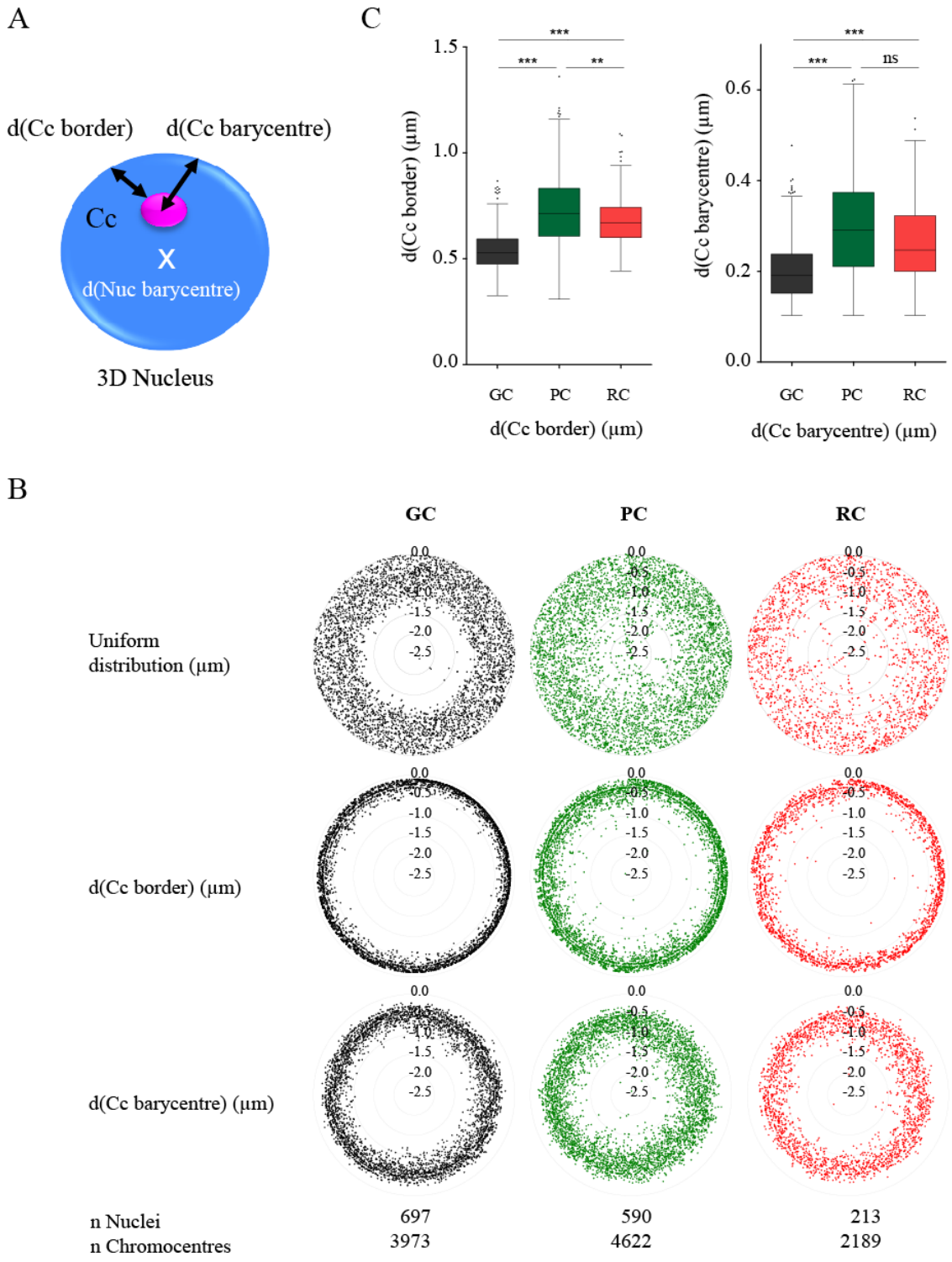
A
d(Cc border)
d(Cc barycentre)
Cc
X
d(Nuc barycentre)
3D Nucleus
C
d(Cc border) (µm)
d(Cc barycentre) (µm)
GC
PC
RC
***
**
ns
B
GC
PC
RC
Uniform distribution (µm)
d(Cc border) (µm)
d(Cc barycentre) (µm)
n Nuclei
n Chromocentres
697
3973
590
4622
213
2189

588

Figure 4

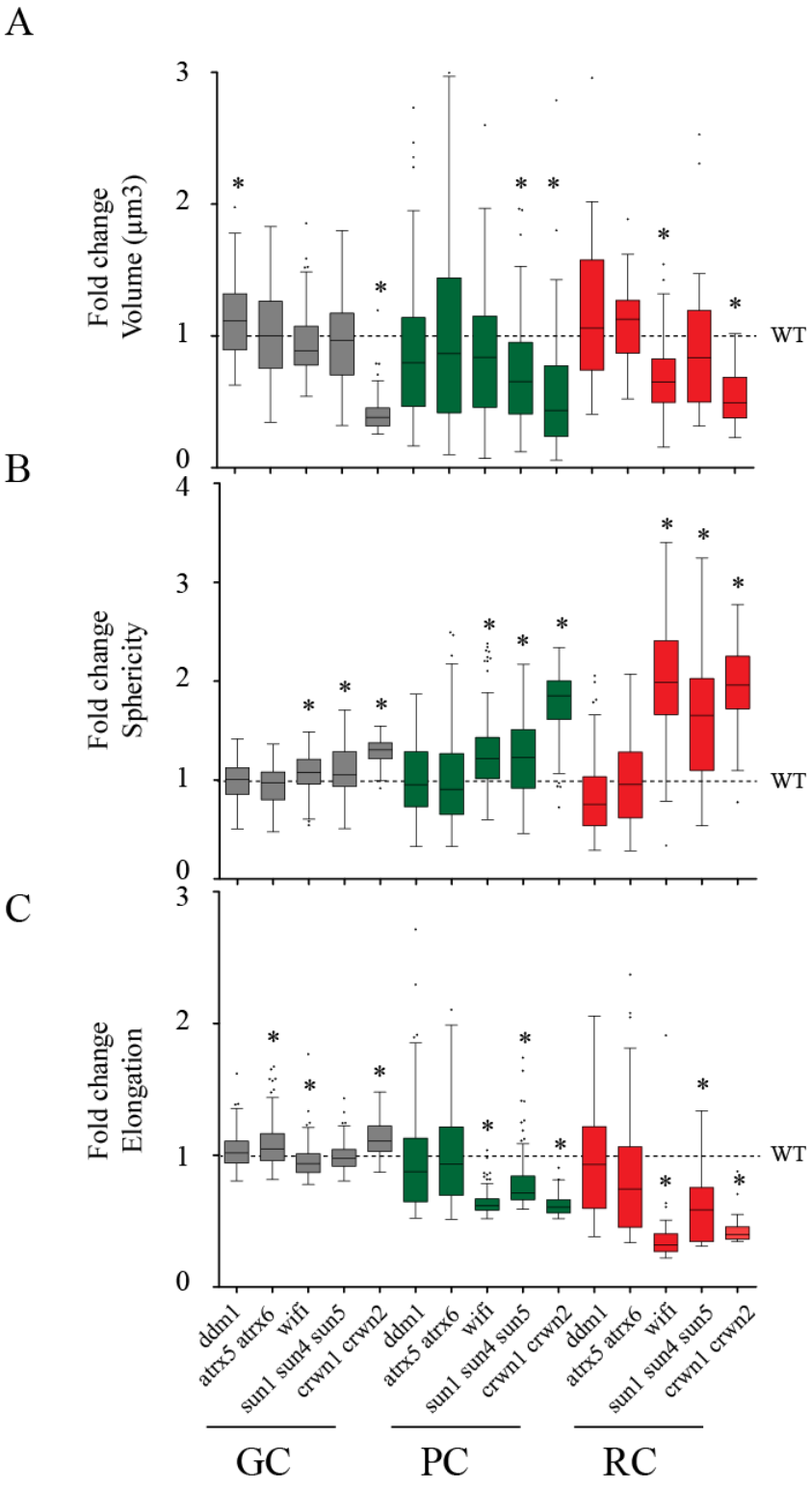
A
B
C
Fold change Volume (µm3)
Fold change Sphericity
Fold change Elongation
WT
ddm1
atrx5 atrx6
wifi
sun1 sun4 sun5
crwn1 crwn2
GC
PC
RC

589

Figure 5

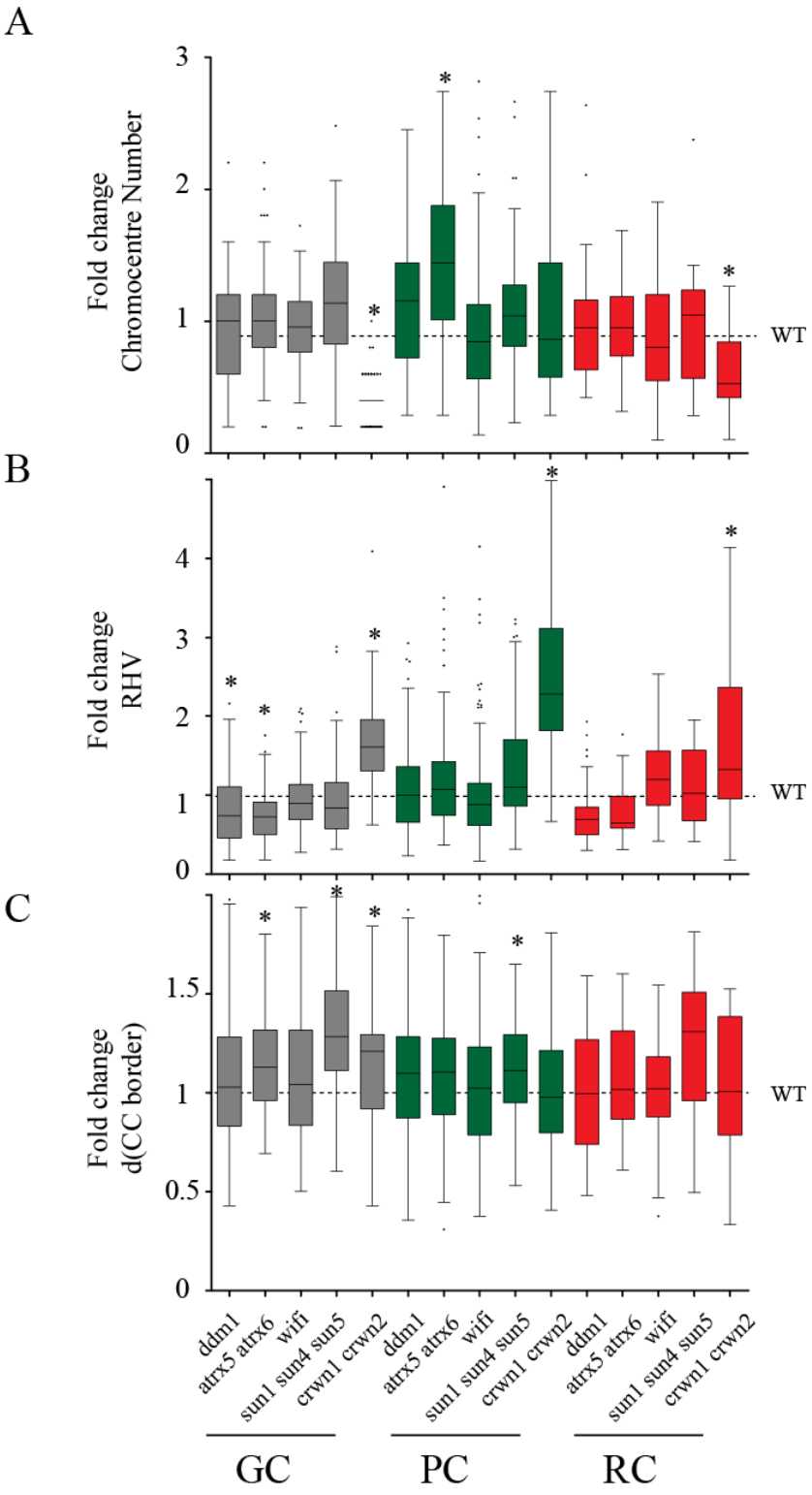
A
B
C
Fold change Chromocentre Number
Fold change RHV
Fold change d(CC border)
WT
ddm1
atrx5 atrx6
wifi
sun1 sun4 sun5
crwn1 crwn2
GC
PC
RC

590

**Figure 6**

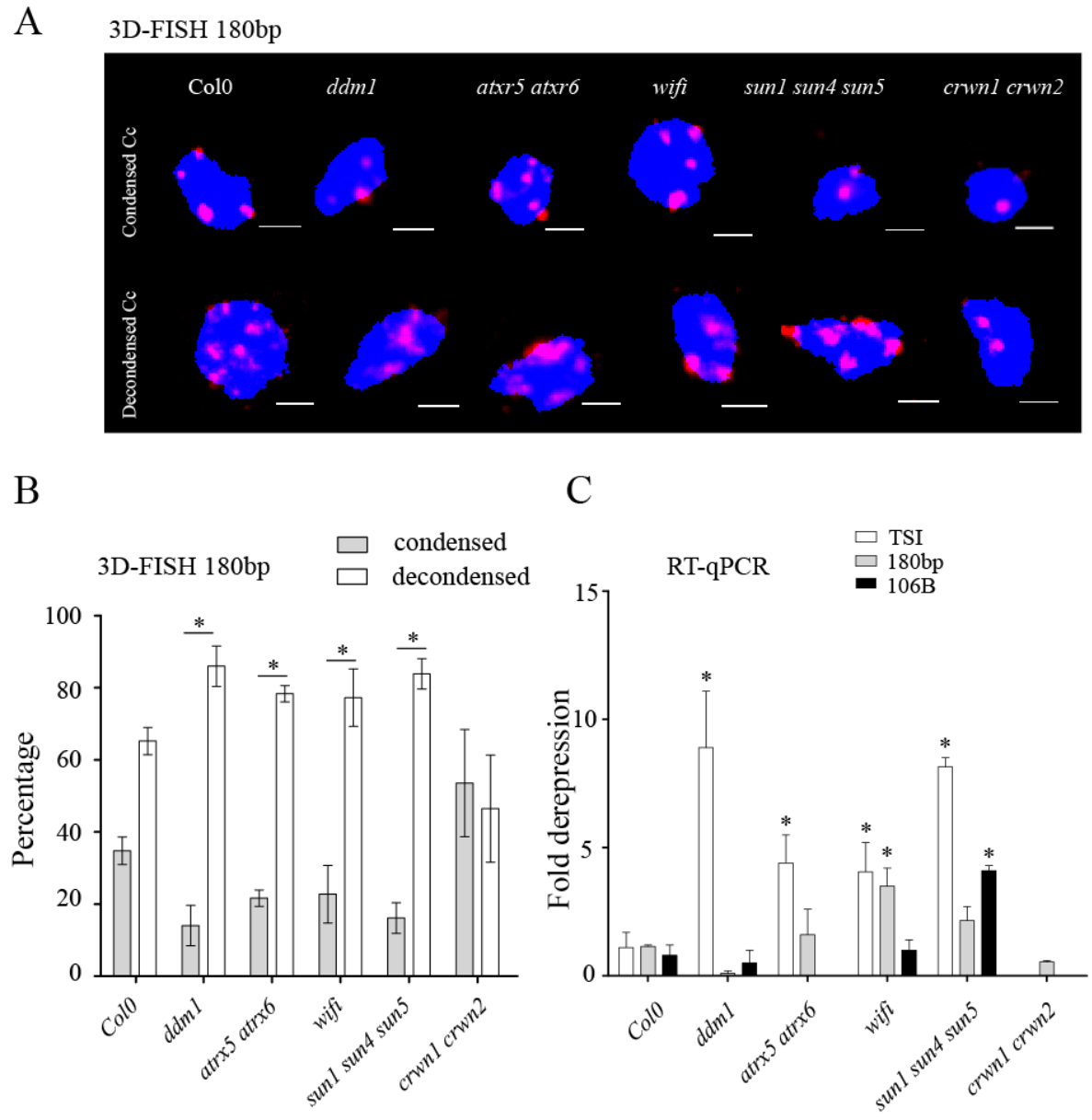
A
3D-FISH 180bp
Col0
ddm1
atxr5 atxr6
wifi
sun1 sun4 sun5
crwn1 crwn2
Condensed Cc
Decondensed Cc
B
3D-FISH 180bp
condensed
decondensed
Percentage
100
80
60
40
20
0
Col0
ddm1
atrx5 atrx6
wifi
sun1 sun4 sun5
crwn1 crwn2
C
RT-qPCR
TSI
180bp
106B
Fold derepression
15
10
5
0
Col0
ddm1
atrx5 atrx6
wifi
sun1 sun4 sun5
crwn1 crwn2

591

**Figure 1**

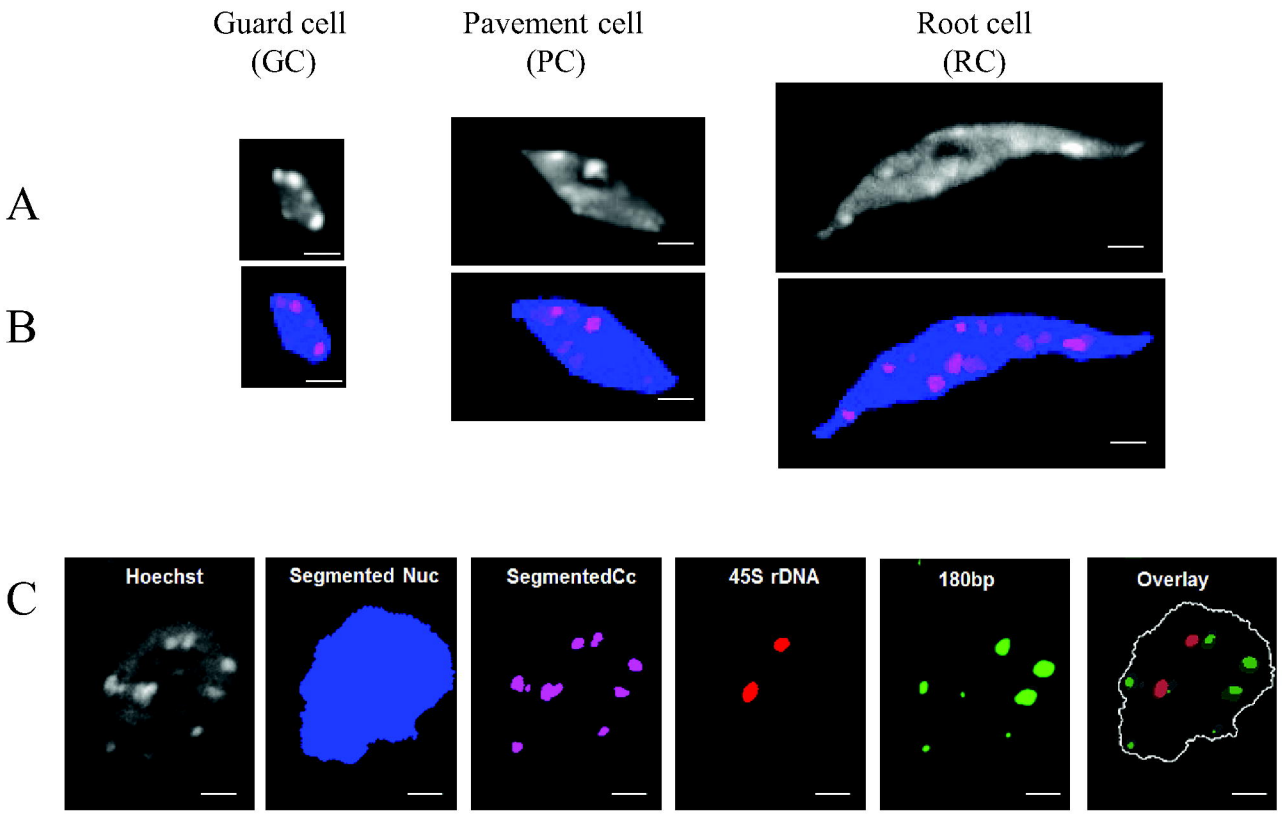
Guard cell
(GC)
Pavement cell
(PC)
Root cell
(RC)
A
B
C
Hoechst
Segmented Nuc
SegmentedCc
45S rDNA
180bp
Overlay

# Figure 2

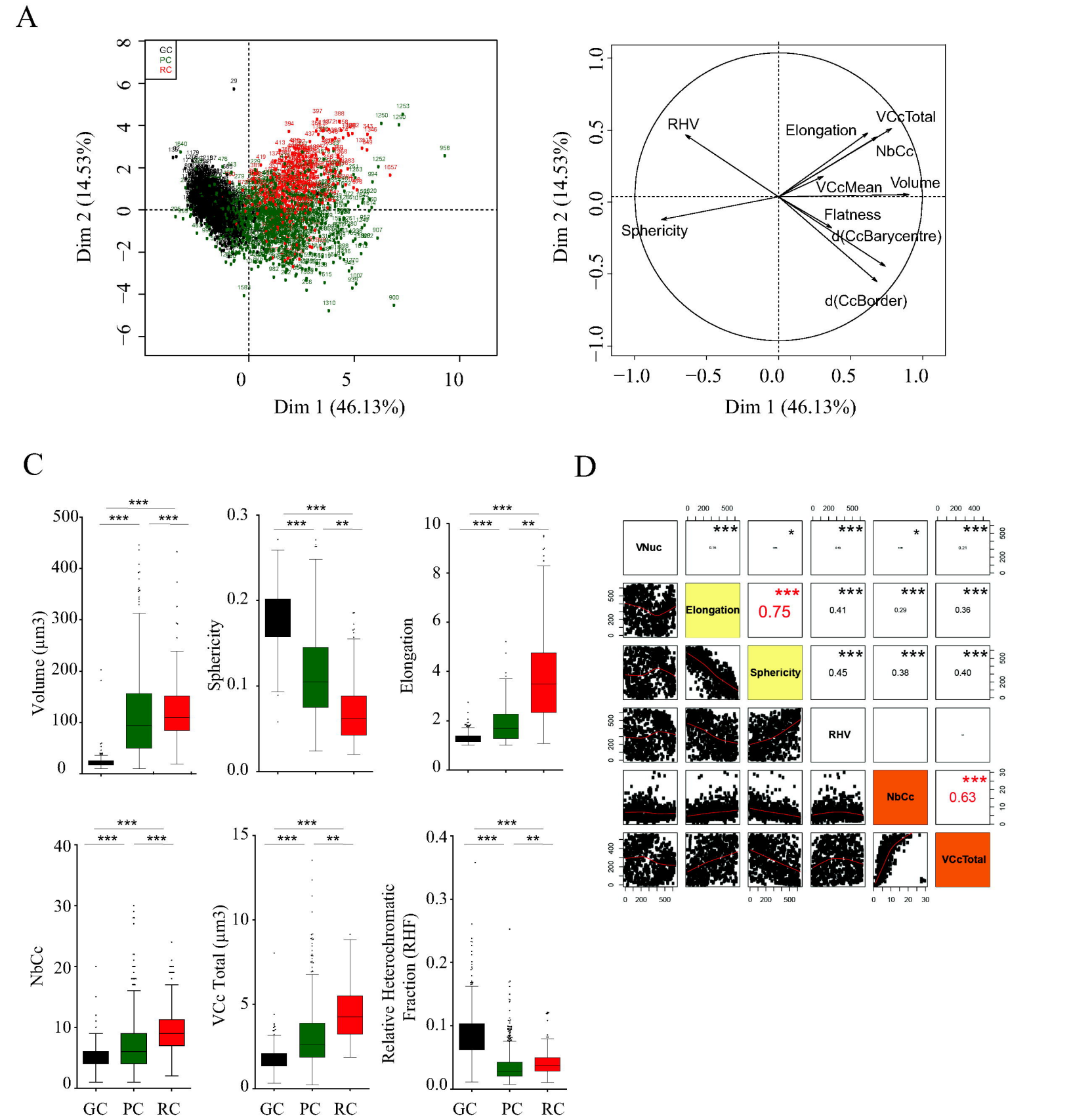
A
GC
PC
RC
Dim 2 (14.53%)
Dim 1 (46.13%)
RHV
Elongation
VCcTotal
NbCc
VCcMean
Volume
Flatness
Sphericity
d(CcBarycentre)
d(CcBorder)
C
Volume (µm3)
Sphericity
Elongation
NbCc
VCc Total (µm3)
Relative Heterochromatic Fraction (RHF)
GC
PC
RC
D
VNuc
Elongation
Sphericity
RHV
NbCc
VCcTotal
0.75
0.41
0.29
0.36
0.45
0.38
0.40
0.63

Figure 3

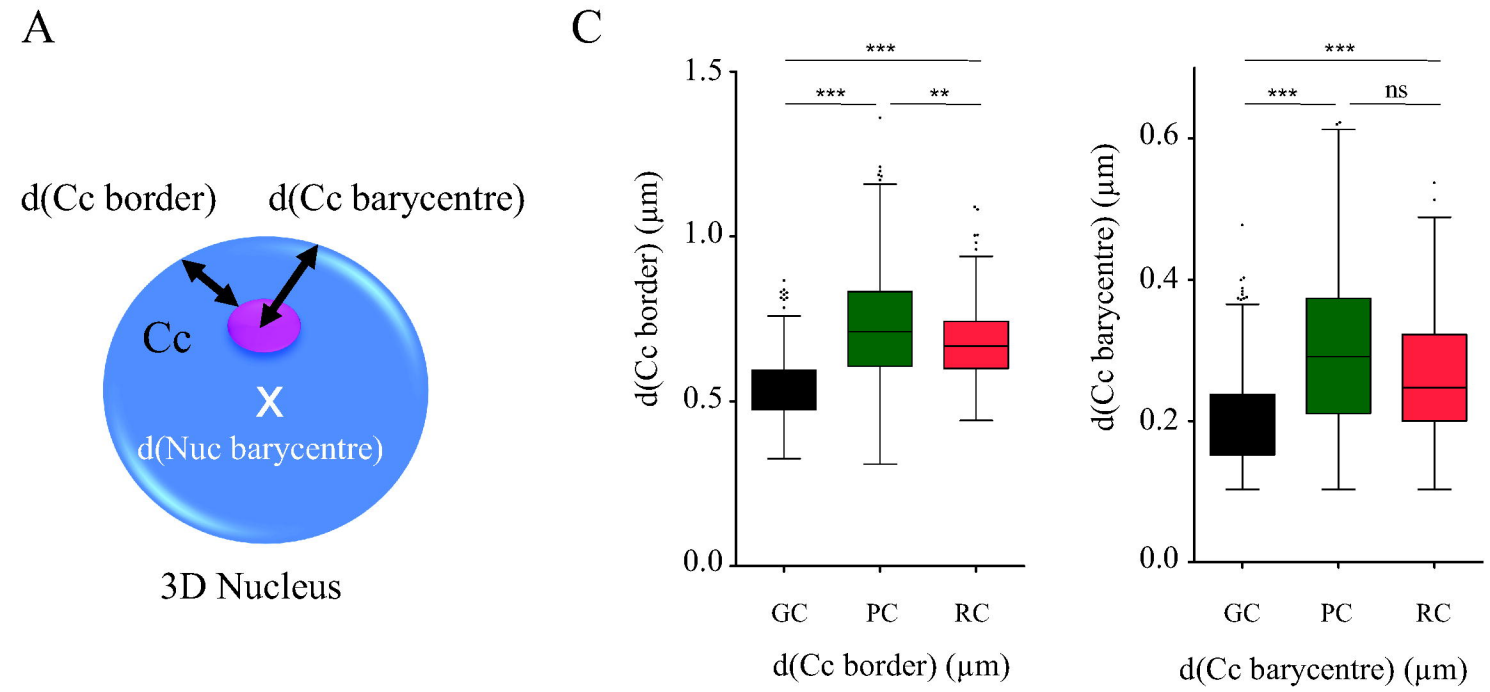
A
d(Cc border)
d(Cc barycentre)
Cc
X
d(Nuc barycentre)
3D Nucleus
C
d(Cc border) (µm)
1.5
1.0
0.5
0.0
***
***
**
GC
PC
RC
d(Cc border) (µm)
d(Cc barycentre) (µm)
0.6
0.4
0.2
0.0
***
***
ns
GC
PC
RC
d(Cc barycentre) (µm)

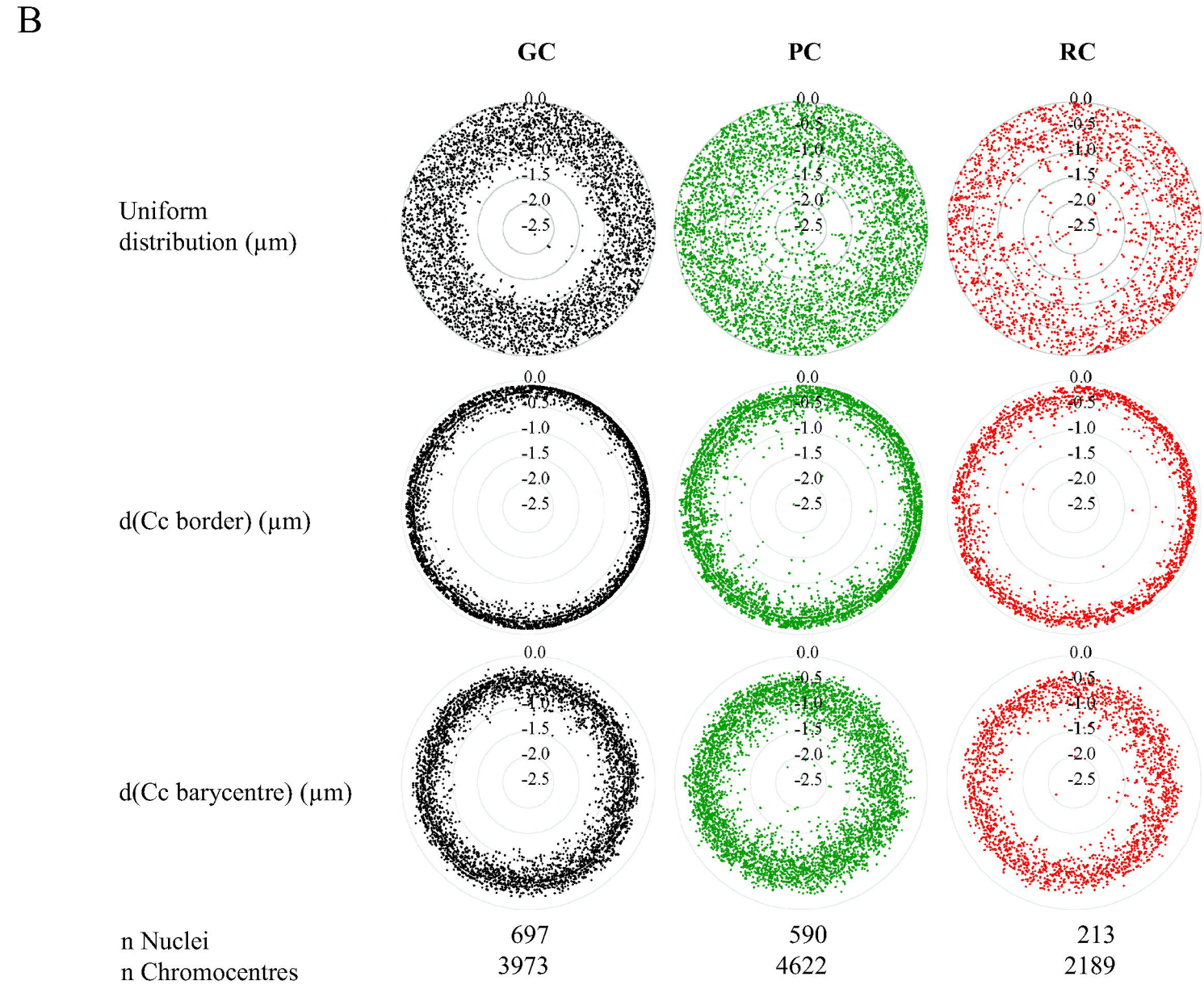
B
GC
PC
RC
Uniform distribution (µm)
d(Cc border) (µm)
d(Cc barycentre) (µm)
0.0
-0.5
-1.0
-1.5
-2.0
-2.5
n Nuclei
n Chromocentres
697
3973
590
4622
213
2189

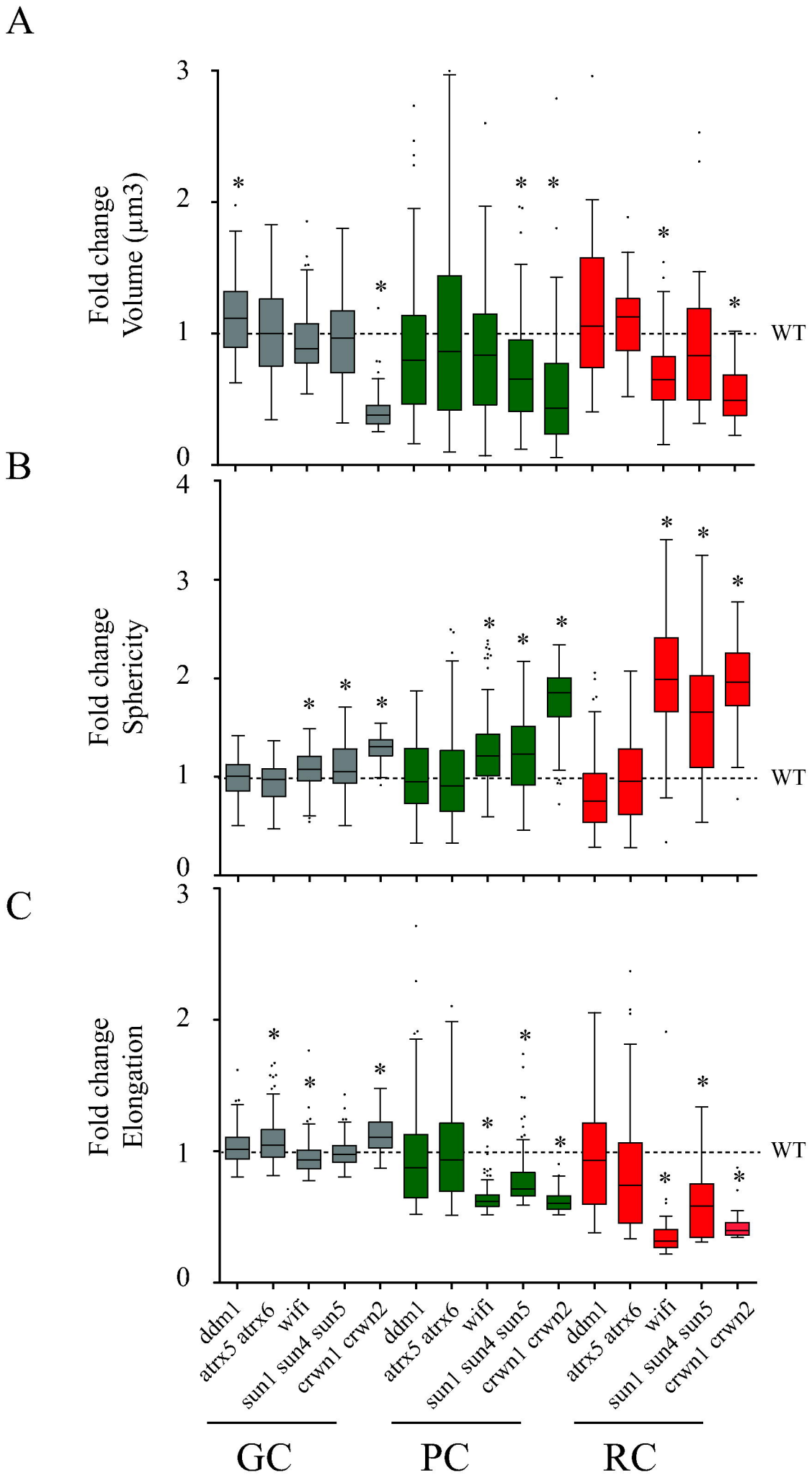
A
B
C
Fold change
Volume (µm3)
Fold change
Sphericity
Fold change
Elongation
WT
0
1
2
3
4
ddm1
atrx5 atrx6
wifi
sun1 sun4 sun5
crwn1 crwn2
GC
PC
RC

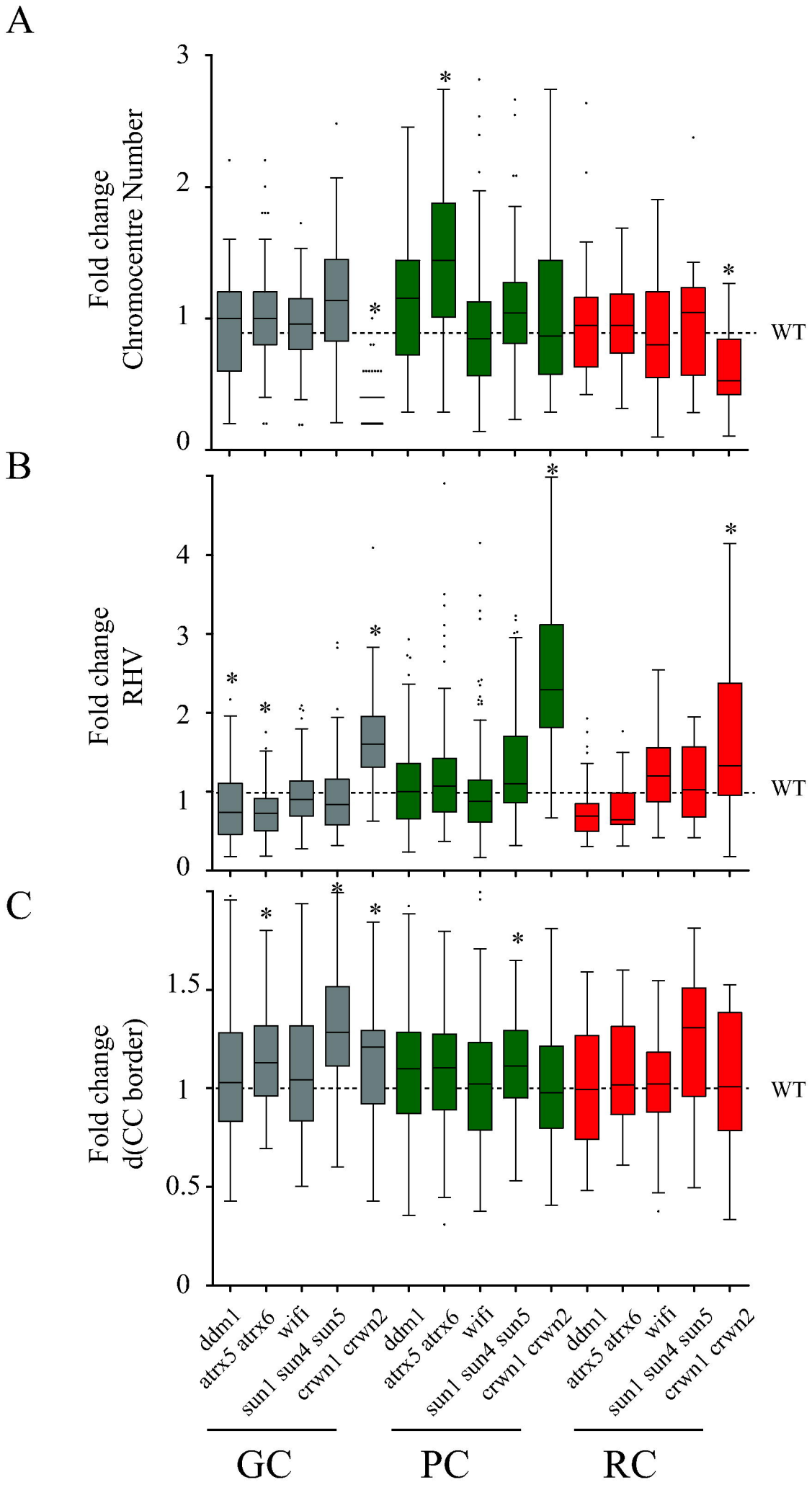
A
Fold change
Chromocentre Number
3
2
1
0
WT
B
Fold change
RHV
4
3
2
1
0
WT
C
Fold change
d(CC border)
1.5
1
0.5
0
WT
ddm1
atrx5 atrx6
wifi
sun1 sun4 sun5
crwn1 crwn2
ddm1
atrx5 atrx6
wifi
sun1 sun4 sun5
crwn1 crwn2
ddm1
atrx5 atrx6
wifi
sun1 sun4 sun5
crwn1 crwn2
GC
PC
RC

**Figure 6**

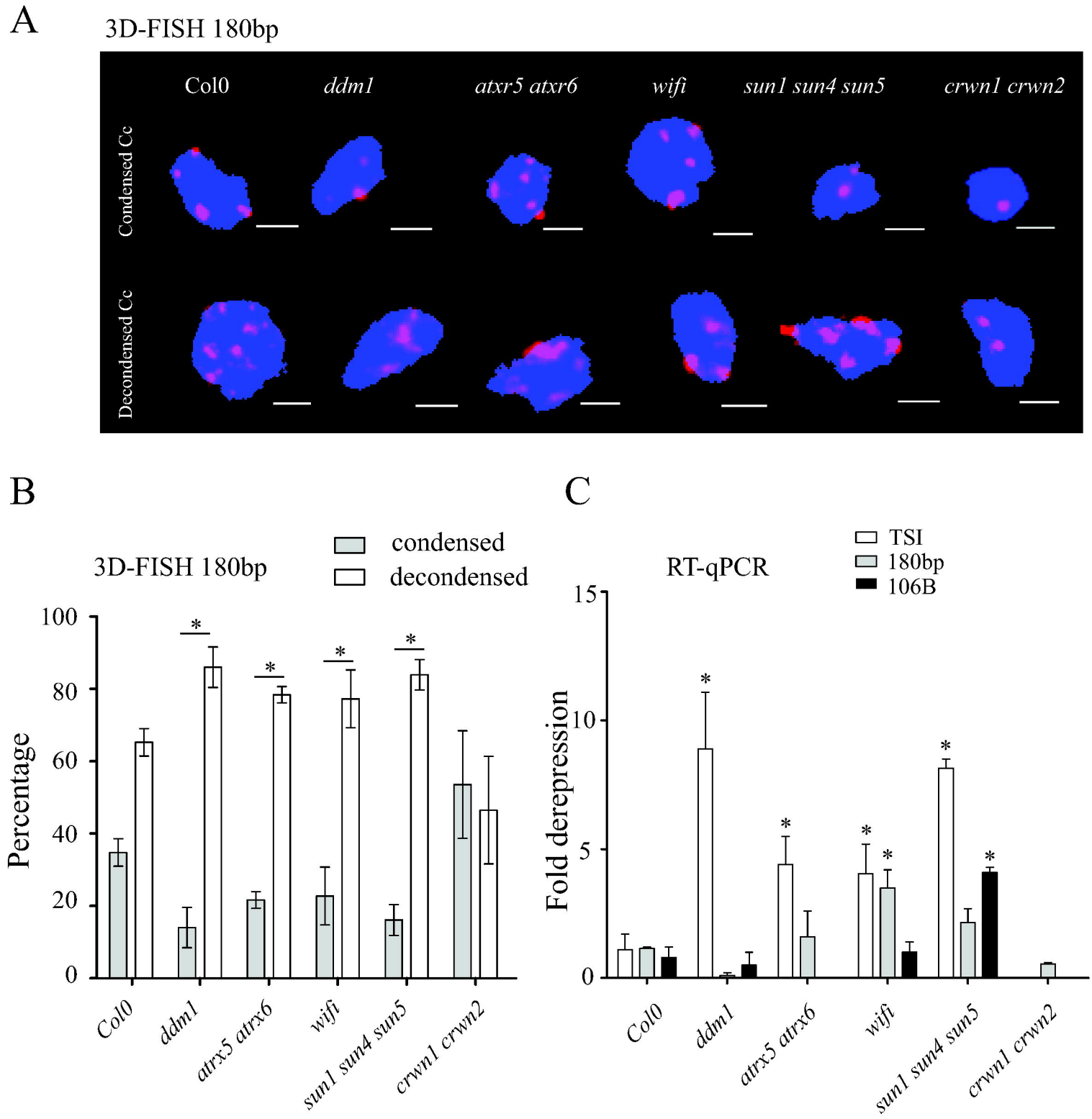
A
3D-FISH 180bp
Col0
ddm1
atxr5 atxr6
wifi
sun1 sun4 sun5
crwn1 crwn2
Condensed Cc
Decondensed Cc
B
3D-FISH 180bp
condensed
decondensed
Percentage
100
80
60
40
20
0
Col0
ddm1
atrx5 atrx6
wifi
sun1 sun4 sun5
crwn1 crwn2
C
RT-qPCR
TSI
180bp
106B
Fold derepression
15
10
5
0
Col0
ddm1
atrx5 atrx6
wifi
sun1 sun4 sun5
crwn1 crwn2